Earth-Science Reviews 198 (2019) 102929

Contents lists available at ScienceDirect

Earth-Science Reviews

journal homepage: www.elsevier.com/locate/earscirev

Airborne lidar change detection: An overview of Earth sciences applications

Unal Okyay[a,*], Jennifer Telling[a], Craig L. Glennie[a], William E. Dietrich[b]

[a] National Center for Airborne Laser Mapping, Department of Civil and Environmental Engineering, University of Houston, 5000 Gulf Freeway, Building 4, Suite 216, Houston, TX 77204-5059, USA

[b] Department of Earth and Planetary Science, University of California, Berkeley, 307 McCone Hall, Berkeley, CA 94720-4767, USA

ARTICLE INFO

Keywords:
Multi-temporal
Airborne laser scanning
ALS
Repeat lidar
Change detection

ABSTRACT

In the last two decades, airborne laser scanning (ALS) has found widespread application and driven fundamental advances in the Earth sciences. With increasing availability and accessibility, multi-temporal ALS data have been used to advance key research topics related to dynamic Earth surface processes. This review presents a comprehensive compilation of existing applications of ALS change detection to the Earth sciences. We cover a wide scope of material pertinent to the broad field of Earth sciences to encourage the cross-pollination between sub-disciplines and discuss the outlook of ALS change detection for advancing scientific discovery. While significant progress has been made in applying repeat ALS data to change detection, numerous approaches make fundamental assumptions that limit the full potential of repeat ALS data. The use of such data for 3D change detection is, therefore, in need of novel, scalable, and computationally efficient processing algorithms that transcend the ever-increasing data density and spatial coverage. Quantification of uncertainty in change detection results also requires further attention, as it is vitally important to understand what 3D differences detected between epochs represent actual change as opposed to limitations in data or methodology. Although ALS has become increasingly integral to change detection across the Earth sciences, the existence of pre- and post-event ALS data is still uncommon for many isolated hazard events, such as earthquakes, volcanic eruptions, wildfires, and landslides. Consequently, data availability is still a major limitation for many ALS change detection applications.

1. Introduction

Rendering Earth's surface in 3D, **Li**ght **D**etection **a**nd **R**anging (lidar), also referred to as laser scanning, has enabled high accuracy mapping of topography, bathymetry, and vegetation. By increasing both the amount and detail of information to an unprecedented level, laser scanning has found widespread application and driven fundamental advances in the Earth sciences. The contributions that laser scanning has delivered across Earth sciences are reflected in the sharply increasing number of publications relying on lidar over the last two decades. Consequently, a number of reviews on laser scanning in specific applications have been published (e.g., Deems et al., 2013 in snow depth measurement; Hodgetts, 2013 in the petroleum industry; Jaboyedoff et al., 2012 for landslide investigation; Tarolli, 2014 for geomorphology; and Wulder et al., 2012 for forest characterization).

Lidar data within the scope of Earth sciences span a wide array of spatial scales ranging from global (satellite), to regional (airborne), to local (terrestrial or mobile). Airborne laser scanning (ALS), in particular, has been widely adopted in Earth science because it provides high accuracy and resolution models that enable quantification at scales previously not possible. The combination of the high resolution, areal coverage, and sub-canopy mapping capability of ALS has revolutionized data acquisition and helped to transform our understanding of the Earth surface (Meigs, 2013; Tarolli, 2014). Consequently, ALS has become a standard tool in many branches of Earth science (Höfle and Rutzinger, 2011). The applications of ALS in Earth science include, but are not limited to, ecology, volcanology, glaciology, hydrology, geomorphology, and active tectonics (e.g., Charlton et al., 2003; Hudnut et al., 2002; Jensen et al., 2008; Kennett and Eiken, 1997; Marenco et al., 2011).

To date, the bulk of studies in Earth science used lidar data from single acquisitions, however, recently the number of studies taking advantage of multi-temporal lidar data has been steadily increasing. The temporal dimension from repeat data acquisitions has provided scientists with new capabilities to detect and evaluate spatiotemporal change. The potential of additional lidar dimensions for advancing change detection was realized early on (e.g., Murakami et al. 1999) and has been highlighted elsewhere (e.g., Eitel et al., 2016). However, a

* Corresponding author.
E-mail addresses: uokyay@central.uh.edu (U. Okyay), jtelling@central.uh.edu (J. Telling), clglenni@central.uh.edu (C.L. Glennie), bill@eps.berkeley.edu (W.E. Dietrich).

https://doi.org/10.1016/j.earscirev.2019.102929
Received 14 November 2018; Received in revised form 30 June 2019; Accepted 16 August 2019
Available online 19 August 2019
0012-8252/

detailed review of ALS change detection as applied to disciplines within the Earth sciences has not been presented. The steady growth in the number of ALS change detection studies is likely to continue with increasing data availability and thus, a review of the state-of-the-art throughout the Earth sciences is timely.

In this review, we cover a wide scope of change detection studies using ALS pertinent to the broad field of Earth sciences, highlighting specific aims, outcomes, and needs to encourage the cross-pollination between sub-disciplines. Providing a comprehensive summary of studies and ideas, this review will come in useful for the growing number of Earth scientists working on ALS change detection in various sub-disciplines. We first give an overview of ALS change detection. We then review existing repeat ALS applications in Earth science, divided by sub-discipline. Finally, we discuss the outlook of ALS change detection for advancing applications and probable future research directions in order to maximize the capabilities of multi-temporal ALS observations. Repeat lidar data acquisition was previously classified by Eitel et al. (2016) as multi-temporal (> 1 month) and hyper-temporal (≤ 1 month), which accounts for more frequent data acquisition intervals such as autonomous TLS. In this review, however, we do not follow this classification and term all repeat ALS data acquisitions as multi-temporal regardless of the return interval.

2. ALS change detection

Remote change detection has become an important tool for monitoring and understanding the dynamic processes of the local and global environment. Singh (1989) referred to remote change detection as the "process of identifying differences in the state of an object or phenomenon by observing it at different times." Remote change detection quantifies the spatiotemporal differences including differences in spectra, position (2D), elevation (2.5D), and volume (3D). With an ever expanding collection of available data, remote change detection will likely continue to be one of the top active research fields in the Earth sciences (Jianya et al., 2008; Zhu, 2017).

Time stacks of imaging data obtained mostly from passive sensors have been used to study and monitor change on Earth's surface for decades (Wulder and Coops, 2014); many passive imaging change detection algorithms have been developed, and a number of literature reviews already exist (e.g., Coppin et al., 2004; Hansen and Loveland, 2012; Lu et al., 2004; Singh, 1989; Zhu, 2017). Providing mostly 2D information, the image-oriented approach by itself is not sufficient for most spatiotemporal change, which is inherently 3D (Qin et al., 2016). To fill this gap, vertical information can only be extracted indirectly from multiple overlapping images using photogrammetry. Laser scanning, on the other hand, expands the scope of change detection applications to a fully 3D space. Consequently, multi-temporal ALS data have been used in many applications such as monitoring changes in coastline (e.g., Meredith et al., 1999) and canopy structure (e.g., Wulder et al., 2012), quantifying mass balance of glaciers (e.g., Geist et al., 2003), and near-field surface deformation (e.g., Ekhtari and Glennie, 2017) to name a few.

The use of repeat ALS data can in many situations provide improved change detection results compared to passive imaging approaches. Because the location of each lidar return point is determined relative to the sensor location in 3D, ALS data from different epochs are not affected by geometric distortion due to perspective, which provides the capability to detect change regardless of the viewing angle. For imaging data, perspective distortion is a major issue and has limited the scope of change detection applications to data acquired with comparable viewing angles (Qin et al., 2016). Furthermore, imaging data acquired using passive sensors are adversely affected by seasonal variations in solar incidence angle. Consequently, images typically need to be selected from the same season or seasonal effects need to be corrected prior to any change detection analysis (Zhu, 2017). A lidar-based approach is more robust in this regard because, unlike passive remote sensing, lidar does not rely on solar radiation and thus, is not affected by ambient illumination conditions or seasonal solar angle differences (Chen et al., 2017).

Another prominent advantage of a lidar-based approach stems from its ability to penetrate small gaps in the canopy making it possible to render the 3D geometry of the underlying topography and detect morphological changes. Observations such as these, conducted through canopy or ground cover, have the potential to significantly advance earthquake, volcanology, and morphodynamics studies, as well as others, where key features may be partially obscured by vegetation. Along with terrain models, canopy height models can be derived from ALS data, which allows for the detection of change in canopy structure and biomass. Therefore, a lidar-based approach is not only well-suited for quantifying morphological change but also for monitoring change in vegetation structure with both high accuracy and level of detail (Campbell et al., 2017).

Despite the numerous advantages that ALS change detection has to offer, a number of limitations remain. Incompatibility between data collections is probably the greatest challenge in utilizing repeat ALS for change detection. Acquisition parameters and scanning systems are often dissimilar between different epochs of data, particularly those with large temporal spacing (e.g., Glennie et al., 2014; Hudak et al., 2012). As a result, the processing, analysis, and interpretation of multi-temporal ALS data become exceedingly complicated without further understanding of how the incompatibilities between data collections should be treated (Eitel et al., 2016).

Acquiring data of appropriate quality is an important step for any change detection application (Lu et al., 2004). The definition of data quality and requirements for different change detection applications can be highly disparate and depend on the scale of the change intended to be resolved (Passalacqua et al., 2015). ALS data quality usually refers to the spatial resolution and positional uncertainty of an individual data collection. Due to a wide variety of available scanning systems and propriety processing algorithms, the positional uncertainties associated with data collections also vary (Qin et al., 2016). Therefore, understanding the potential error sources and recognizing error budgets for individual data collections is crucial for lidar change detection (Deems et al., 2013). For instance, inadequate system calibration and/or improper spatial error modeling of individual data collections introduce substantial systematic errors and adversely influence change detection analysis (Glennie et al., 2014). Furthermore, ALS sensors record laser returns without prejudice; the generated point cloud may contain points from manmade structures, vegetation, or underlying topography. It is, therefore, necessary to differentiate and classify ground and above-ground returns. This process, however, introduces classification uncertainty, depending on the methodology employed, and is made complex by the presence of vegetation and topographic complexity. Inaccuracies in ground vs above-ground return classification may result in apparent change regardless of whether or not real change has taken place. Therefore, positional and classification uncertainties collectively influence the applicability, quantitative accuracy, and informative values of ALS change detection. While understanding and accounting for these uncertainties is important, it is currently not considered in most change detection applications using laser scanning, and a detailed discussion is beyond the scope of this paper. Passalacqua et al. (2015) offers an intensive discussion on common sources of error leading to uncertainties in lidar data and derived products, spatial modeling of these uncertainties, and error propagation.

Although ALS is regarded as a reliable source for point data with high positional accuracy, horizontal and vertical accuracy are not uniform. According to Glennie (2007), a good rule-of-thumb for ALS data is that the vertical accuracy is almost 5 times better than the horizontal accuracy. Currently, the best case positional (vertical/horizontal) accuracy of ALS data is about 0.05/0.2 m and 0.15/0.6 m at 500 m and 3000 m flight altitude, respectively (Glennie, 2007; Passalacqua et al., 2015). The resolution of ALS data is commonly

discussed based on point density (number of points per m^2) and is determined by flight and sensor parameters (Renslow, 2012; Shan and Toth, 2008). It is common for the point density of ALS data to vary between different epochs of data. The typical point density of modern ALS data varies between 1 and 30 points per square-meter whereas for legacy data (i.e., from before roughly 2007) it is around 0.1 to 2 points per square-meter (Passalacqua et al., 2015). Owing to advances in scanning systems, ALS has provided increasingly higher positional accuracy and point density over time (Wulder et al., 2012). The increase in point density could cause apparent changes in bare-earth topography that is only due to greater penetration through vegetation and more highly resolved features. Consequently, it is usually the older legacy data that limits the accuracy and quality of change detection analysis. Another important aspect pertinent to data compatibility is co-registration of different epochs of data. Proper georeferencing of the pre- and post-event data with consistent projections and datums is fundamental to any further analysis (Passalacqua et al., 2015). Improper (or missing) georeferencing and registration of data collections prevents proper alignment of the pre- and post-event data. In the absence of proper co-registration it becomes unclear whether the analysis results represent real change or simply an artifact related to the misalignment between data collections (Glennie et al., 2014).

3. Multi-temporal ALS in Earth sciences

In the last two decades, the use of multi-temporal ALS data has dramatically increased and a variety of methodologies have been implemented to elucidate fundamental earth surface processes. Below, we briefly address commonly used ALS change detection methods and present a comprehensive summary of the existing repeat ALS applications for the biosphere, cryosphere, and geosphere. The biosphere is defined to include those processes that impact the intersection between the critical zone and the broader field of ecology, including biomass calculations and wildfire response studies. The cryosphere is defined as those studies relating specifically to snow and ice, whether they be in the Arctic, the Antarctic, or elsewhere around the world. Finally, the geosphere encapsulates the sub-disciplines that typically fall under the broader definition of geology i.e. volcanology, surface deformation, morphodynamics, and landslides.

Some of the most commonly used methods within the scope of Earth sciences are Differencing of DEMs (DoD) (Wheaton, 2008), Iterative Closest Point (ICP) (Besl and McKay, 1992), Particle Image Velocimetry (PIV) (Keane and Adrian, 1992), and Co-registration of Optically Sensed Images and Correlation (COSI-Corr) (Leprince et al., 2007). Beyond these commonly used methods, a number of ALS change detection methods tailored for specific applications and purposes have been proposed. Due to their limited use, these methods are briefly addressed in their respective sections below.

DoD and ICP have been, by far, the most frequently used methods in repeat ALS change detection studies. DoD is a simple image-based method to quantify changes in elevation between different epochs of lidar-derived DEMs. In the DoD approach, the elevations of an older DEM are subtracted from a new DEM on a pixel-by-pixel basis. Using the grid size and elevation differences obtained from DoD, volumetric changes over time can be estimated. As such, Wheaton et al. (2010) suggested that the DoD can be used to detect and quantify any volumetric changes larger than the minimum detection limits. ICP is a rigid body transformation that minimizes the point to point differences between two point clouds. The algorithm matches the closest points in the reference (non-moving) point cloud to those in the target (moving) point cloud and then estimates the rotation and translation required to minimize the point to point distances throughout the point cloud. The target points are then transformed and the point to point distances are recalculated. The algorithm runs iteratively until the misregistration error between the two point clouds falls below a user-defined threshold.

PIV is an image registration method developed in the fluid dynamics community. The original technique relied on particles, seeded in fluids, to track the motion of the fluid flow. This method has since been adapted for image analysis, where individual pixels can be treated similarly to particles seeded in a fluid. In order to use the PIV method, lidar data must first be converted to an image. In most Earth science applications, the image is colorized based on elevation. The primary advantage of the PIV technique is that it provides a non-rigid transformation, which is necessary for accurately modeling many Earth science phenomena, for example landslides. COSI-Corr is another image-based method developed specifically for monitoring surface deformation. The method allows precise co-registration and sub-pixel-correlation of temporally spaced images. Sub-pixel correlation of pre- and post-event images, achieved by phase plane correlation in the Fourier domain, reveals the horizontal displacement due to surface deformation. While the method was initially developed for optical imagery, it has since been used for lidar-derived DEMs elevation models and laser intensity images. Like PIV, COSI-Corr provides non-rigid transformation parameters allowing accurate horizontal deformation estimations.

3.1. Biosphere

3.1.1. Above-ground biomass (AGB)

While single ALS data collections have been used to estimate AGB stock, multi-temporal ALS allows for modeling AGB change over time. Approaches for modeling AGB change using repeat ALS can be separated into direct and indirect approaches (McRoberts et al., 2014, 2015). The indirect approach models the AGB using laser metrics at two points in time and estimates the change in AGB as the difference between these models. The direct approach uses the difference in the laser metrics over time to estimate the change in AGB as a single model. Implementing an indirect approach, Hudak et al. (2012) quantified AGB change and carbon flux in the heavily managed, mixed conifer forests of Moscow Mountain, ID. Using in-situ measurements and laser metrics in a Random Forest machine learning algorithm (Crookston and Finley, 2008), predictive AGB models were created to estimate biomass change at the plot, pixel, and landscape levels (Fig. 1). The results indicated a net gain in AGB across the non-harvested forest and a net loss across harvested forests. Overall, Moscow Mountain was found to be a carbon source rather than a sink. It has been also noted that, despite a 30-fold point density difference, plot-scale AGB change estimations were not affected because the ALS data of different epochs were used to model AGBs independently. The AGB stock and change in biomass across a typical Mediterranean woodland, located in central Spain, was assessed in an indirect modeling approach (Simonson et al., 2016). Regression models on the basis of lidar-derived mean canopy height and in-situ AGB estimates were created and used to estimate AGB stock and biomass change over time. The lidar-derived and in-situ AGB change estimates were found to be in a close agreement. The results were then used to simulate AGB dynamics over the next 100 years. The findings suggested that AGB accumulation was accelerating, making the investigated forest a carbon sink under undisturbed conditions.

Tropical peat swamp forests in Indonesia have been huge natural pools for carbon. However, due to deforestation and forest degradation they have recently become a source of carbon. Biomass change in a peat swamp forest near Sabangau, Central Kalimantan, was evaluated by implementing an indirect approach (Boehm et al., 2013). The forest regrowth and peat subsidence were estimated using lidar-derived Canopy Height Models (CHMs) and in-situ measurements. Between 2007 and 2011 the peat swamp subsided 18 cm whereas the forest regrew 1.9 m suggesting the study area exhibits balance in the absence of logging (Boehm et al., 2013). Another peat swap forest in Central Kalimantan near Plangka Raya was studied and the AGB dynamics were quantified using an indirect approach with a focus on unaffected, burned, and selectively logged forests (Englhart et al., 2013). The results indicated that 92% of the total biomass was lost across the burned

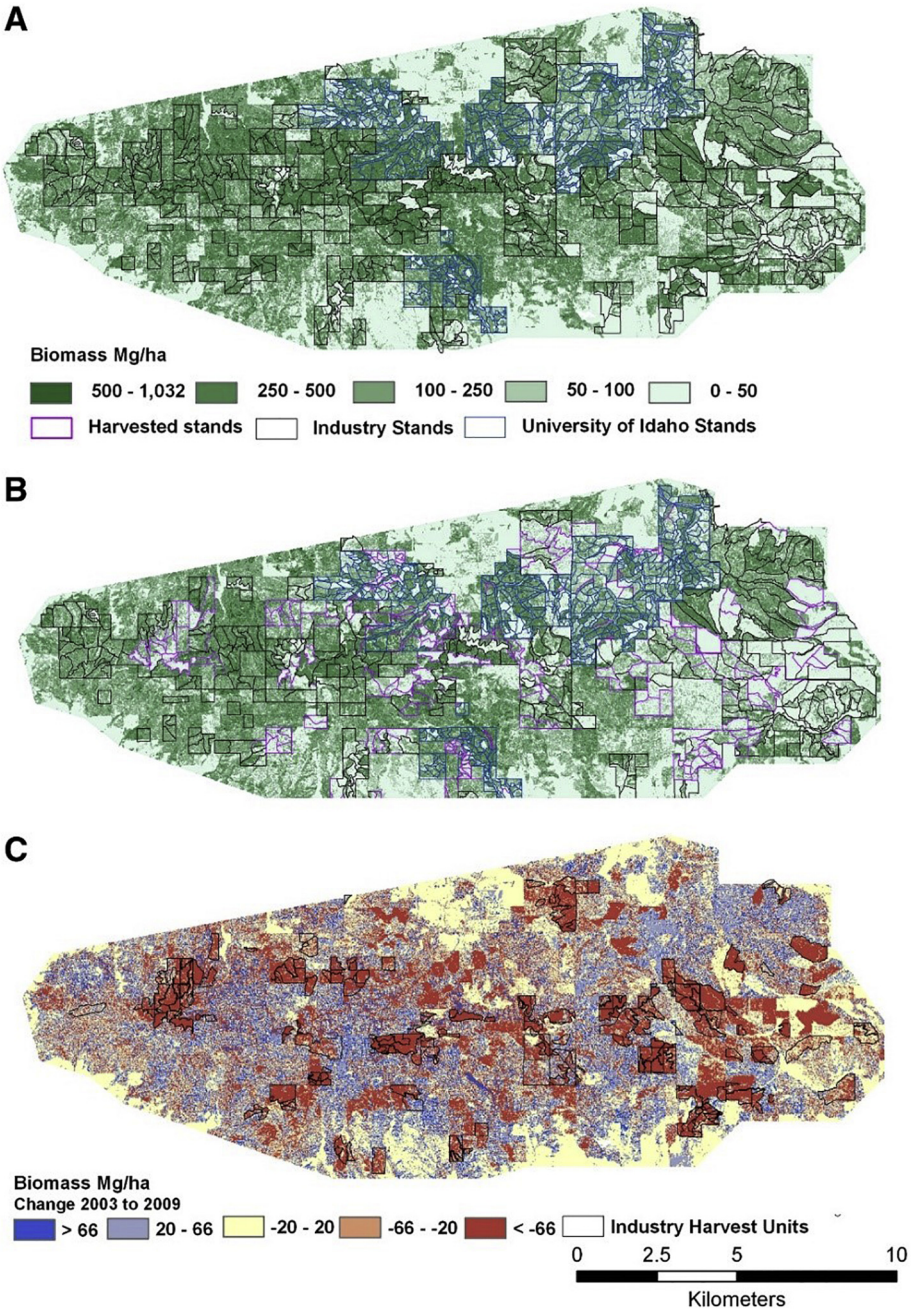

Fig. 1. Predicted AGB across the study area in Moscow Mountain, ID in (A) 2003 and (B) 2009. (C) Estimated AGB change obtained differencing (A) and (B). Figure originally from Hudak et al. (2012), used with permission.

forests. Unaffected forests exhibit a net biomass gain and canopy height growth whereas selectively logged forests exhibit a net loss despite the observed canopy height growth. While logging is an important pathway to deforestation and increased carbon emission, the amount of carbon release remains uncertain as the affected areas and carbon loss as a result of logging have not been well quantified. In one such study, Andersen et al. (2014) evaluated AGB changes associated with low-density logging in natural tropical forests in the Western Brazilian Amazon. Regression models were created and AGB change estimates were obtained by differencing predictor rasters. The findings indicated that the entire area exhibited a net AGB loss but the biomass loss in areas affected by logging was almost six fold that of unaffected areas.

Monitoring changes in high-biomass tropical forests using ALS poses specific challenges due to the significantly higher AGB modeling errors. Nevertheless, a few studies have sought to evaluate AGB dynamics in tropical forests using repeat ALS data. The change in AGB over a period of four years was evaluated in an old-growth tropical forest of French Guiana (Réjou-Méchain et al., 2015). In-situ AGB measurements were regressed against lidar-derived median canopy height for 0.25 and 1 ha areas to obtain AGB estimates. The change in AGB over time was estimated by differencing these models and was subsequently compared to in-situ AGB change estimates. The results showed a weak correlation between in-situ and lidar-derived estimates, which is only significant at the 0.25 ha resolution, and suggested that AGB dynamics of old-growth tropical forests are not directly comparable from ground and lidar perspectives. Similar findings concerning AGB dynamics in tropical forests were reported in other literature (Dubayah et al., 2010). Canopy structure and AGB dynamics across the tropical forests of the La Selva Biological Station in Costa Rica were evaluated in an experimental study using full waveform ALS data (Dubayah et al., 2010). Adopting a

direct approach, changes in laser metrics were related to in-situ AGB change observations for a series of old-growth and secondary forests. However, the model performance was found to be weak. Nevertheless, AGB change over the seven-year study was mapped at 1-ha resolution using the plot level relationships. The results indicated a net loss of height but no net AGB change in old-growth forests, whereas secondary forests exhibited net height growth and net AGB gain. These results were then used to infer whether old-growth and secondary forests were sources, neutral, or sinks in terms of carbon flux. Secondary forests were found to be predominantly sinks or neutral whereas old-growth forests host spatially distributed sources and sinks.

While many studies implemented only one modeling approach, a few studies evaluated the accuracies of both direct and indirect approaches in estimating AGB change. The magnitude and spatial pattern of AGB change in an old-growth tropical forest on Barro Colorado Island, Panama was evaluated using both the indirect and direct approaches at different spatial scales (0.04–10 ha) (Meyer et al., 2013). The results indicated higher uncertainties associated with the direct modeling approach for both AGB stock and biomass change estimates at spatial scales smaller than 10 ha. While the indirect modeling approach resulted in accurate estimates of AGB stock at 1 ha resolution, accurate AGB change estimates were obtained at 10 ha resolution. Thus, regardless of the modeling approach, repeat ALS estimated changes in AGB with acceptable accuracy for areas larger than 10 ha. The finding indicated old-growth forests exhibit a net loss of AGB, whereas the secondary forests exhibit a net gain across the study area over 10 years. It was also shown that there are no advantages to estimating AGB change at spatial scales comparable to crown sizes, and that, in fact, spatial scales below 1 ha are dominated by uncertainties. Cao et al. (2016) analyzed AGB change over a period of six years across a mixed subtropical forest (Yushan Forest) near Suzhou, China using both indirect and direct modeling approaches. The results indicated that direct modeling produced better AGB change estimates compared to the indirect approach. The spatial analysis of modeled AGB change has shown that the investigated forest exhibits a net biomass gain over a six year period and that the rate of biomass gain varied with respect to forest type and age.

Bollandsås et al. (2013) evaluated different approaches for modeling biomass change on 52 reference plots in a mountain forest near Ringebu, Norway. In addition to the commonly used indirect and direct approaches, a modified direct approach based on the relative annual growth rate in the AGB was tested. The results indicated the superiority of direct approaches over the indirect approach, while the traditional direct approach performed slightly better than the modified direct approach. Økseter et al. (2015) compared the accuracy of direct and indirect approaches for estimating biomass change in 39 circular reference plots of a young boreal forest near Valer, Norway. In addition to the three approaches evaluated in Bollandsås et al. (2013), two additional direct modeling variants were tested. As opposed to Bollandsås et al. (2013), the findings indicated the indirect approach produced the best results across the study area for a wide range of forest conditions. The same data used in Økseter et al. (2015) were also used in Næsset et al. (2013), Næsset et al. (2015), and McRoberts et al. (2015). The direct and indirect approaches were compared in a statistically rigorous and analytically derived, model-assisted estimation of AGB change (Næsset et al., 2013). The findings indicated that direct modeling performed better for estimating mean biomass change over time when compared to the indirect approach. Næsset et al. (2015) evaluated the effect of plot size on model-assisted direct and indirect estimation of AGB change. Likewise, the direct AGB estimation approach produced better relative efficiency compared to the indirect approach. The results also showed a positive correlation between relative efficiency and increasing plot size, indicating that plot size is an important survey design parameter that should be taken into account for precise remote AGB estimation. In addition to model-assisted direct and indirect approaches, McRoberts et al. (2015) used simple random sampling for estimating AGB change. As previously reported in the literature, both direct and indirect model-assisted approaches were found to be superior to simple random sampling. However, unlike the previously reported findings, the indirect model-assisted approach produced more accurate AGB change estimates in the study area. Model-assisted direct and indirect modeling approaches for estimating AGB change were tested in a 3×3 km plot in the Silas Little Experimental Forest in New Lisbon, NJ (Skowronski et al., 2014). The results favored the direct modeling approach for estimating biomass change over time. It was also shown that a model-assisted indirect approach revealed larger variances compared to in-situ biomass change estimations obtained from simple random sampling; whereas a model-based direct approach produced a smaller variance compared to in-situ estimations.

3.1.2. Wildfire response

ALS has been used sparingly to examine and characterize the effects of wildfire in a dynamic way (Alonzo et al., 2017; Bohlin et al., 2017; McCarley et al., 2017b; Reddy et al., 2015). While post-wildfire, single ALS data can be used to estimate changes to forest volume, tree canopy cover, and other metrics, these products are improved through the use of complementary pre- and post-wildfire ALS datasets (McCarley et al., 2017a; Reddy et al., 2015). New products characterizing the effects of wildfires can also be developed where repeat ALS data are available, including measurement of surface layer removal (Alonzo et al., 2017) and tree-fall following wildfire events (Bohlin et al., 2017). Finally, when other multi-temporal products, such as Landsat data, share a coverage area with repeat ALS data, variable burn rates for individual tree species (McCarley et al., 2017b) or for specific levels of tree health (McCarley et al., 2017a) can be determined.

A combination of multi-temporal ALS and Landsat data were used to examine the 2005 Fox Creek wildfire, in the Kenai Peninsula, AK (Alonzo et al., 2017), the 2002 House River fire, in Alberta, Canada (Wulder et al., 2009), and the 2012 Pole Creek fire, outside of Bend, OR (McCarley et al., 2017b). In all three of these studies, there was pre- and post-fire Landsat and ALS data coverage of the affected area. Landsat data is frequently used to assess pre- and post-fire forest conditions, including structure, burn severity and normalized burn ratio, and to measure the changes in canopy cover resulting from wildfire (Alonzo et al., 2017; Wulder et al., 2009). Wulder et al. (2009) used the two data types in a primarily complementary way where ALS data was used to specifically look at vertical forest structure, which is used to estimate wildfire carbon emissions, inter-tree distance, and crown closure. A marked increase in inter-tree distance and a decrease in canopy closure were observed in the ALS data when comparing post-fire data to pre-fire data. ALS and Landsat metrics, including crown closure, vegetation fill, and change in canopy height for ALS and normalized burn ration for Landsat, were found to be more closely correlated in the post-fire data than the pre-fire data, an important consideration for any forest evaluation.

Repeat ALS and Landsat data over the Pole Creek, OR, wildfire were used to assess what areas of the forest can be most accurately captured by lidar, when compared to spectral Landsat data (McCarley et al., 2017b). Generally speaking, the study found that canopy assessments could be clearly made using lidar but that, depending on the density and structure of the forest, there was less agreement between lidar and Landsat results lower in the forest structure. A second study of the same fire, using the same datasets, specifically examined the effect that pine beetles have on the spread and severity of wildfire (McCarley et al., 2017a). Trees that had been affected by the pine beetle outbreak experienced a higher degree of burn severity, which is defined as the amount of lost organic matter (Keeley, 2009), and a greater loss of canopy material than those that were not affected. A different repeat ALS and Landsat study examined the 2005 wildfire on the Kenai Peninsula, AK (Alonzo et al., 2017). Pre-fire data from both ALS and Landsat were used to classify tree types and then these classifications were used to analyze burn severity in the post-fire data. Vegetation type

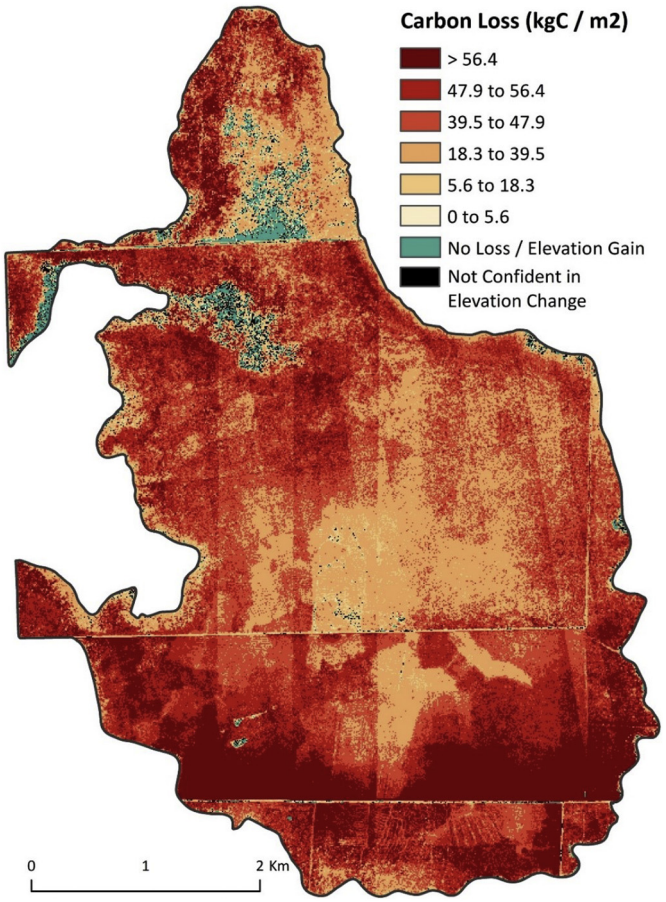

Fig. 2. Estimated carbon loss per m^2 as a result of the 2011 Great Dismal Swamp National Wildlife Refuge, VA wildfire. Figure originally from Reddy et al. (2015), used with permission.

and location were both found to have a controlling influence on burn severity but, in general, vegetation type alone was the stronger indicator. Black spruce in upland areas lost markedly less canopy material than the same species did in flat, lowland areas. However, white spruce saw the same degree of canopy loss regardless of terrain. Broadleaf trees, overall, experienced the least reduction in canopy volume following the fire. The study results are instructive for understanding the heterogeneous effects of forest fire and could also be helpful in predicting forest fire severity in areas at high risk for forest fires.

Rather than examining the more commonly used metrics, including burn severity, fire intensity, tree canopy loss, and forest density, for wildfire, a wildfire study in Sweden used repeat ALS to measure the degree of tree-fall following the fire (Bohlin et al., 2017; Keeley, 2009). Combined with training data collected in the field, the study was able to model the degree of tree-fall with relative success. Post-fire carbon release was the focus of a peat bog fire study in the Great Dismal Swamp National Wildlife Refuge, VA (Reddy et al., 2015). Repeat ALS data allowed for the accurate assessment of burned volume in an area that would have been difficult to characterize with discrete in-situ measurements (Fig. 2). Despite the burned area being far less than that in other peat wildfires, the carbon released per unit of area was notably higher because a combination of dry conditions and anthropogenic damming resulted in a drier than normal peat bog at the onset of the fire.

3.2. Cryosphere

Multi-temporal ALS data have been used to improve our characterization of glacial advance and retreat (Geist et al., 2003; Joerg et al., 2012; Knoll and Kerschner, 2009), glacier volumetric changes (Bollmann, 2010; Hopkinson and Demuth, 2006), snow water equivalent based on snow fall volume (Painter et al., 2016; Schöber et al., 2014), and glacier detection (Kodde et al., 2007), among other applications.

One of the most common applications of repeat ALS data in the cryosphere is to define glacial extents and quantify the retreat and advance of glaciers and associated parameters, such as volumetric changes. In regions with numerous, smaller glaciers, tracking the evolution of individual glaciers can be challenging (Abermann et al., 2010; Knoll and Kerschner, 2009). Knoll and Kerschner (2009) used ALS data, in conjunction with previously collected orthophotographs, to identify and measure areal changes in eight separate glacier groups in South Tyrol, Italy, and noted the importance of high resolution ALS data in regions with multiple, smaller features. A different study in the same region of Italy examined four ice glaciers and one rock glacier with four ALS scans taken between 2001 and 2006 (Abermann et al., 2010). The goal of the study was to determine how accurately glacier boundary changes could be defined using ALS when compared to other common methods. Despite sampling variable glacier surfaces, including both debris free and debris rich surfaces, in the study, the results showed that high resolution ALS data significantly improved the accuracy with which glacial extents could be defined and noted that this was especially true for smaller glaciers.

A study of Hintereisferner glacier in Austria and Engabreen glacier in Norway collected seasonal ALS data over the course of two years (Geist et al., 2003). Though the changing extent of the glaciers was measured, minimal differences were noted from one year to the next. However, the high frequency of data collection in the study enabled a seasonal evaluation of glacier surface features, such as crevasses, and the study was able to track the lifecycle of numerous glacial morphological features with high precision. A much longer study, running from 2001 to 2008, used inter-annual ALS data to analyze the accuracy of glacial volumetric calculations, when compared to other common methods, and to calculate the mass balance of Hintereisferner glacier in Austria (Bollmann, 2010). ALS had a notable advantage over other methods, such as the direct glaciological method, which requires in situ measurements on the glacier surface, due to the higher resolution of the ALS data, which captures small scale surface variations with far more accuracy. The results of determining glacial volume from ALS varied significantly against those of other techniques but the ALS results were generally determined to be more accurate. The area and volume calculations were used to compute mass balance for Hintereisferner glacier but the use of a single ice density value in these calculations introduced error. A classification scheme based on the intensity of the ALS return pulses was used to estimate zones of varying ice density, refining the mass balance calculations.

Ice loss, especially with a focus on where on the glacier the loss is occurring from, is frequently a focus of ALS research in the cryosphere (Hopkinson and Demuth, 2006; Joerg et al., 2012). Ice loss from a glacier in the Swiss Alps, Findelengletscher, was the target of repeated ALS collections between 2005 and 2010 (Joerg et al., 2012). Given the improvements in ALS technology over the course of the study, a detailed assessment of error was completed prior to any other calculations. The glacier location, on the bottom of a valley, and other attributes, such as its gentle slope and relatively debris-free surface, kept on-glacier errors low throughout the study period. However, a dramatic decrease in off-glacier error, mostly along the steep valley walls, was observed from the beginning of the study to the end. Even including error considerations, the ALS based results indicated far more ice loss from the glacier over the five year study than did in situ measurements taken during the same time frame. The differences were attributed to the difference in resolution between the ALS and in situ data. However, it is worth noting that, while this study (Joerg et al., 2012) showed a consistent under-estimation of ice loss by in situ methods, the study by Bollmann (2010) showed that in situ measurements could either over-

or underestimate volumetric losses, depending on where the in situ data was gathered. A study in the Canadian Rocky Mountains also focused on ice loss from glaciers. However, the study focus was on the downstream water resources (Hopkinson and Demuth, 2006). Two ALS datasets collected two years apart were used to analyze ice loss from Peyto glacier, Canada. Peyto glacier was determined to contribute roughly 16% of the drainage basin's water and the ALS data was used to show that the ice loss was significant from both above and below the snow line, which is defined as the border between a region covered by snow and a region not covered by snow.

While a number of studies have noted that ALS data is helpful in manually locating and characterizing glaciers, Kodde et al. (2007) published a technique for automating the detection and changing characteristics of glaciers in repeat ALS data (Kodde et al., 2007). The method is based on a smoothness criteria that assumes that the glacier surface is relatively smooth in contract to the surrounding terrain and was successfully tested on Hintereisferner glacier, Austria. In addition to detecting the glacier extent, the study also proposed a technique for detecting crevasses automatically, though this identification also relied on certain glacier surface characteristics. Combining these two methods with repeat ALS collections provides an automated method for detecting glacial advance or retreat and for analyzing the changing surface morphology of glaciers. A different dynamic application used repeat ALS data to define the flow field across glacier surfaces using PIV (Telling et al., 2017). In situ studies can only collect a finite number of data points on the glacier surface and flow fields for the glacier are extrapolated based on these points. Telling et al. (2017) showed that PIV can be used on rasterized ALS (or TLS) point clouds to define glacial flow with far higher resolution than in situ methods. However, the study also found that this method only works on glaciers with certain roughness characteristics, since surface features need to be present and clearly defined for the algorithm to track them, and with appropriate data temporal spacing, dependent on the average velocity of the glacier.

Trends in snow accumulation and melt are an important component of water modeling, especially as changing climatological trends alter precipitation patterns (DeBeer and Pomeroy, 2010; Painter et al., 2016; Schöber et al., 2014). Repeat ALS surveys have been used in the Rocky Mountains, North Basin and Range, and the Sierra Nevada Mountains, to track seasonal snowfall accumulation with respect to topography and vegetation (Tennant et al., 2017). In general, increasing snow depth with increasing elevation was noted at all the study sites; however, the relationship was not linear and a sharp drop in snow depth was noted at the highest study elevations. In vegetated areas, both topography and aspect (directional orientation of the slope) were found to exert a secondary influence on snow depth but above the tree line only aspect was found to exert much influence (Tennant et al., 2017). As repeat ALS is increasingly used to monitor snow depth, there is a need to understand the sources of error that may be inherent in these measurements, when compared to in situ data (Tinkham et al., 2014). This study, conducted at Reynolds Mountain, ID, found that snow depth derived from repeat ALS surveys was lowest in low-lying areas with smaller vegetation and highest near forest margins where rapidly changing winds created rapidly varying snow depths.

Building off of snow depth measurements, research at the intersection of the cryosphere and water resources fields translates this data into snow water equivalent (SWE) estimates that can be used in melt water modeling (DeBeer and Pomeroy, 2010; Painter et al., 2016; Schöber et al., 2014). One such study paired bare-earth ALS data with ALS and imaging spectrometer data to both accurately measure the snow depth and to characterize snow albedo (Painter et al., 2016). The total snow volume was calculated from the ALS data, the snow density was estimated based on the snow albedo, and then both measurements were combined to derive SWE (Fig. 3). A similar study was conducted in the Austrian Alps though, in this case, repeat ALS scans were paired with Landsat data to estimate the snow density (Schöber et al., 2014). The SWE results were also used in hydrological models of the study area. Good agreement between the ALS data and the model results was seen at the basin scale but there was less agreement between the two at finer resolutions. A study in Alberta, Canada, used repeat ALS snow depth measurements as the primary input for a model of SWE and melt water scenarios (DeBeer and Pomeroy, 2010). When the model results were compared to in situ observations, it was determined that variable snow pack densities, and correspondingly variable melt rates, were most accurate in replicating the field observations.

3.3. Geosphere

3.3.1. Volcanology

The use of repeat ALS data is still relatively novel in the field of volcanology and limited work has been done exemplifying its utility. Behncke et al. (2016) used repeat ALS data to measure the difference in lava flow volumes between the 2007 and 2010 eruptive episodes of Mt. Etna, Italy. The goal of the study was to estimate total erupted volume, a key parameter in many volcanic models. While the volume was calculated to be approximately $86 \times 10^6\,m^3$, nearly 90% of which was from lava flows, the long lapse between observations enabled some eruptive material to be removed by erosion. The calculated volumes are, therefore, a constraint on the minimum erupted volume between 2007 and 2010. An earlier study of Mt. Etna used multiple overpasses over the course of two days to increase the temporal resolution and capture volcanic activity as it progressed (Favalli et al., 2010a). The high temporal resolution allowed for the quantification of lava pulsing during the eruption, a process that has been observed previously but is difficult to measure. Similar pulsing at all six channels, in different vent zones, led to the conclusion that, at least for the 2006 eruptive event, the pulses were a result of changing material fluxes in the central volcanic conduit.

ALS can also be very useful for assessing morphometric changes to volcanoes. At Mt. Etna, four ALS surveys were conducted between 2004 and 2006 in order to monitor scoria cone growth (Fornaciai et al., 2010). The focus was on the atmospheric and situational factors that led to the deterioration of one scoria cone and the preservation of the other. Two ALS DEMs collected in 2005 and 2007 were used, together with aerial photogrammetry from 1986 and 1998, in order to estimate changes to the summit height and size of Mt. Etna (Neri et al., 2008). A substantial increase in elevation both on and around the volcano was found though the ALS data was noted to be, by far, the more accurate data collection technique, permitting more precise measurements of change between 2005 and 2007.

Monitoring lava flows and evaluating the topographical controls on them is another area that has benefited from repeat ALS (Favalli et al., 2010b; Harris et al., 2010; Joyce et al., 2009). One of Mt. Etna's lava flows was mapped in both 2004 and 2005 using ALS with the goal of observing the evolution of lobes in the flow (Favalli et al., 2010b). Though eight progressing lobes were initially identified in the flow, the outer lobes were observed to become levees, exerting control on the flow motion, over time, rather than remaining active elements of the advancing lava flow. Repeat ALS, in addition to satellite data, was used to map lava flows following the 2007 break-out event at Mt. Ruapehu, New Zealand (Joyce et al., 2009). The study found that manual flow mapping was more precise than any of the automated techniques attempted. However, the ALS data were collected at a low resolution of only 1–2 points per m^2 resulting in a high vertical uncertainty that occasionally exceeded the flow depth, making these areas impossible to identify with the DoD approach. A different study at Mt. Etna used ALS data collected in 2004 and 2006, along with a host of estimated variables regarding flow temperature and viscosity, to calculate the time averaged discharge rate of two lava flows (Harris et al., 2010). The final goal of the project was to make these calculations using repeat satellite overpasses, which are collected at lower cost, but ALS was used to verify and calibrate the satellite technique.

Finally, Favalli et al. (2009) proposed a way to use repeat ALS

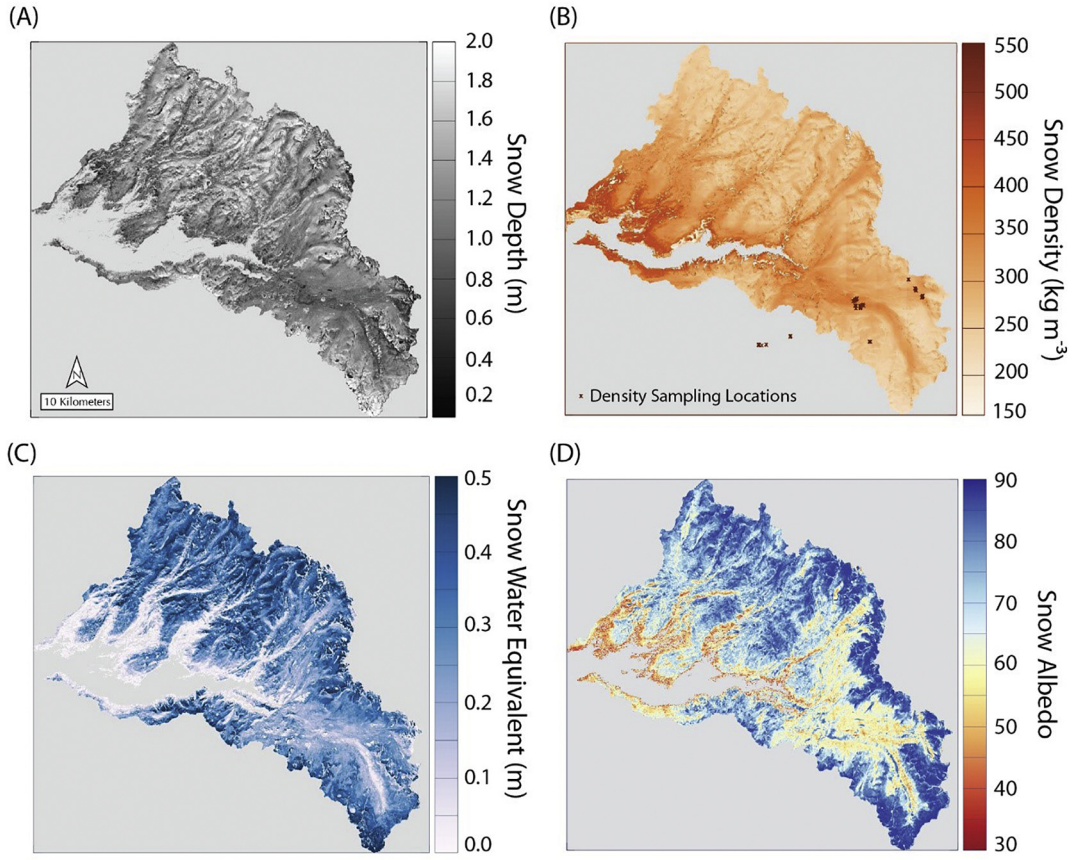

Fig. 3. Snow depth, density, water equivalent, and albedo products as derived from repeat ALS data. Figure originally from Painter et al. (2016), used with permission.

collections specifically for registering data in volcanic settings. While the method itself is used to register strips of a single ALS campaign to one another, the intended final use of such a technique is to monitor change at a smaller scale than would otherwise be feasible with more standard registration techniques. The technique uses multiple tie points in every overlapping area to match features with similar shapes within a small radius on overlapping flight lines. The three-dimensional shift between the features in two overlapping strips provides the registration information (Fig. 4). While the method was tested on ALS data covering Mt. Etna, Italy, it could be used in any application that has sufficient surface roughness.

3.3.2. Surface deformation

Post-event ALS data have proven successful for delineating surface ruptures and for discrete measurement of fault slip along a rupture (e.g., Engelkemeir and Khan, 2008; Hudnut et al., 2002; Meigs, 2013). Spatially distributed coseismic surface deformation, especially in the near-field (< 1 km) of the fault zone, however, cannot be measured directly on the post-event data (Glennie et al., 2014). Repeat ALS collections, on the other hand, provide the ability to render the surface deformation through the comparison of detailed pre- and post-event topography.

DoD, a straightforward method for surface deformation detection, was successfully used to quantify the vertical displacement caused by the 2010 El Mayor – Cucapah, Mexico earthquake (Oskin et al., 2012); the 2010 Darfield, New Zealand earthquake (Duffy et al., 2013); and the 2016 Kaikoura, New Zealand earthquake (Clark et al., 2017). The differential survey of the El Mayor – Cucapah earthquake by Oskin et al. (2012) studied the near-field deformation using a lower-resolution (5 m/pixel) DEM pair. Differential elevation changes revealed significant, spatially distributed vertical displacement in the near-field surrounding the faults. Duffy et al. (2013) used differential analysis of multi-temporal ALS to estimate decimeter-scale deformation across the Waterford releasing bend. Temporal elevation differences highlighted otherwise indiscernible yet important structures and the overlapping nature of the fault segments across the releasing bend. In a recent study, Clark et al. (2017) investigated coseismic coastal deformation caused by the Koikoura earthquake. The differential elevation changes revealed highly variable (−2.5 to 6.5 m) vertical displacement along a ~110 km coastline caused by a rather complex rupture along a transpressional plate boundary. All three studies noted that simple DEM differencing neglects the horizontal displacement and that the apparent vertical change obtained using this method does not necessarily reflect the true vertical displacement. Surface deformation, indeed, occurs along an arbitrary direction in 3D and differential elevation changes stem from both vertical and horizontal motion (Mukoyama, 2011). In an attempt to minimize the effect of lateral motion on vertical displacement estimates, Clark et al. (2017) restricted their analysis to low-slope (< 5°) areas in both pre- and post-event DEMs. The horizontal displacement, however, was not explicitly investigated or quantified. Duffy et al. (2013) performed a sub-pixel correlation of the DEMs using COSI-Corr to estimate horizontal displacement independently. Although pixel correlation revealed a north-northwest-striking structure, it was rather ambiguous on the DoD map and was not detected in the field at all. Pixel correlation was found to be noisy due to the limited extent of the data and the lack of quality correlation points across the area.

Image-based methods, such as COSI-Corr and PIV, have proven successful in quantifying horizontal surface deformation and thus, are getting more attention in the literature. Using PIV on ALS-derived slope maps, Mukoyama (2011) extracted the horizontal vector components of the surface deformation caused by the 2008 Iwate-Miyagi, Japan

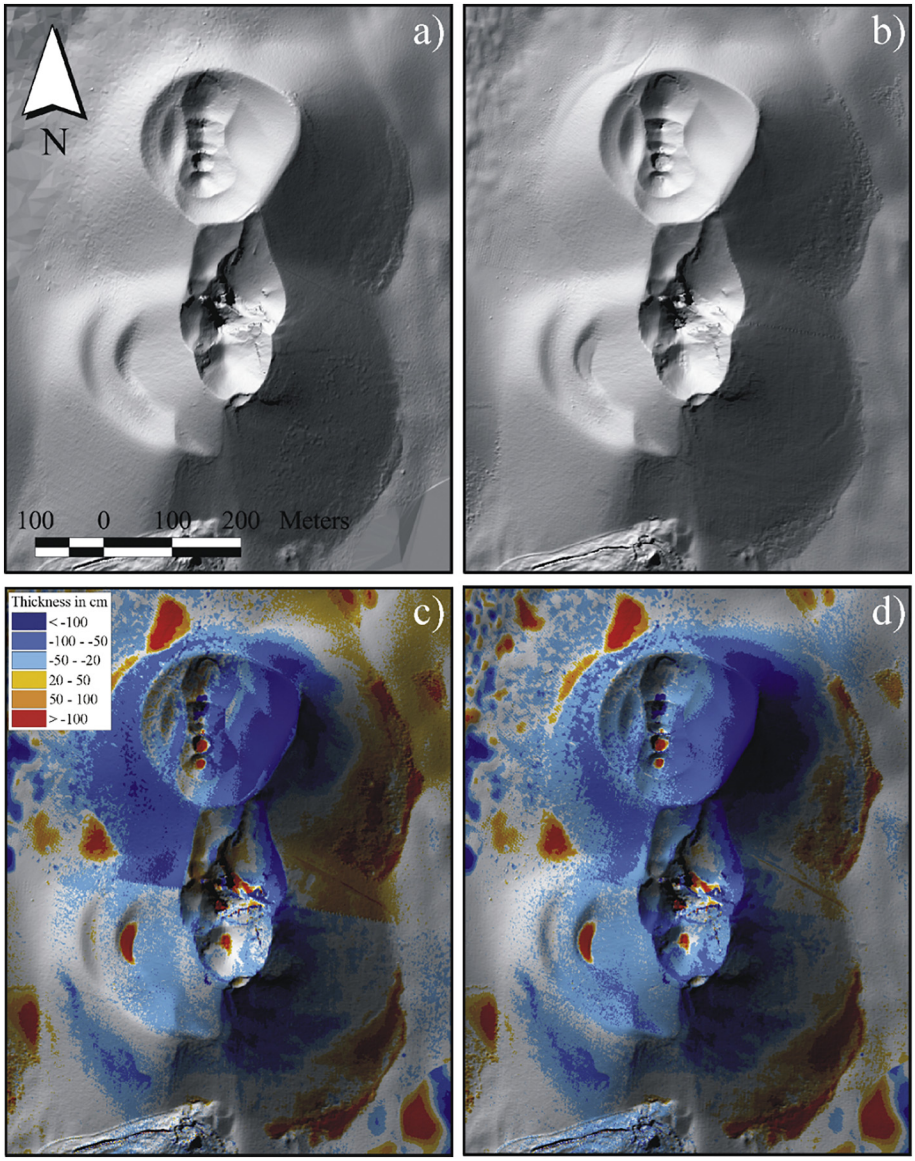

Fig. 4. Corrected DEMs from (a) 2004 and (b) 2005 ALS data. DoD between 2004 and 2005 (c) with the uncorrected and (d) with the corrected DEMs. Figure originally from Favalli et al. (2009), used with permission.

earthquake. The image matching results revealed horizontal displacement ranging between 0.5 m and 5.2 m in varying directions in the investigated area. The vertical components of the deformation vectors were also estimated on the basis of elevation differences at the head and terminal vertices of the vector, revealing a more complete picture of surface deformation. Similarly, Lyda et al. (2016) assessed the surface deformation caused by the 2014 South Napa, CA earthquake using PIV on the lidar-derived DEMs. Horizontal displacement estimates obtained from PIV were comparable to field measurements. In addition to commonly used bare earth elevation models, they analyzed an elevation model that included manmade structures (termed as geodetic markers) in an effort to improve the PIV result. However, including the geodetic markers in PIV improved the results only marginally. Later on, Ekhtari and Glennie (2017) estimated the horizontal displacement in the same study area from laser intensity images using COSI-Corr (Fig. 5). Correlation of ALS intensity images was found to be a successful technique for determining horizontal displacement in vegetated areas. Leprince et al. (2011) estimated the horizontal deformation caused by the El Mayor – Cucapah, Mexico earthquake using ALS-derived DEMs and COSI-Corr. These estimates were then used to compensate for the horizontal offset between the pre- and post-event DEMs, which allowed for an unbiased estimation of vertical displacement using DoD.

All three of the methods discussed so far require gridding of ALS data and thus, the surface deformation estimates are inherently 2.5D at best. ICP, on the other hand, allows direct estimation of surface deformation in 3D. In fact, ICP and its variants have been the primary method for estimating spatially distributed, 3D surface deformation from either irregularly-spaced point clouds or regularly-gridded elevation models. Nissen et al. (2012) was the very first to demonstrate the potential of ICP to estimate 3D surface deformation. The method was tested on pre-earthquake and synthetically deformed post-earthquake point clouds. The post-event data collection was simulated from the "B4" (Bevis et al., 2005) ALS survey of the San Andreas Fault near Coachella, CA. They show that the described adaptation of ICP not only reproduced the simulated deformation, with around 20 cm horizontal and 4 cm vertical accuracy, but also allowed measurement of the rotation directly from the point clouds.

Nissen et al. (2014) estimated surface deformation caused by the 2008 Iwate-Miyagi and 2011 Fukushima-Hamadori earthquakes by applying an adaptation of ICP to gridded, digital terrain models. In both

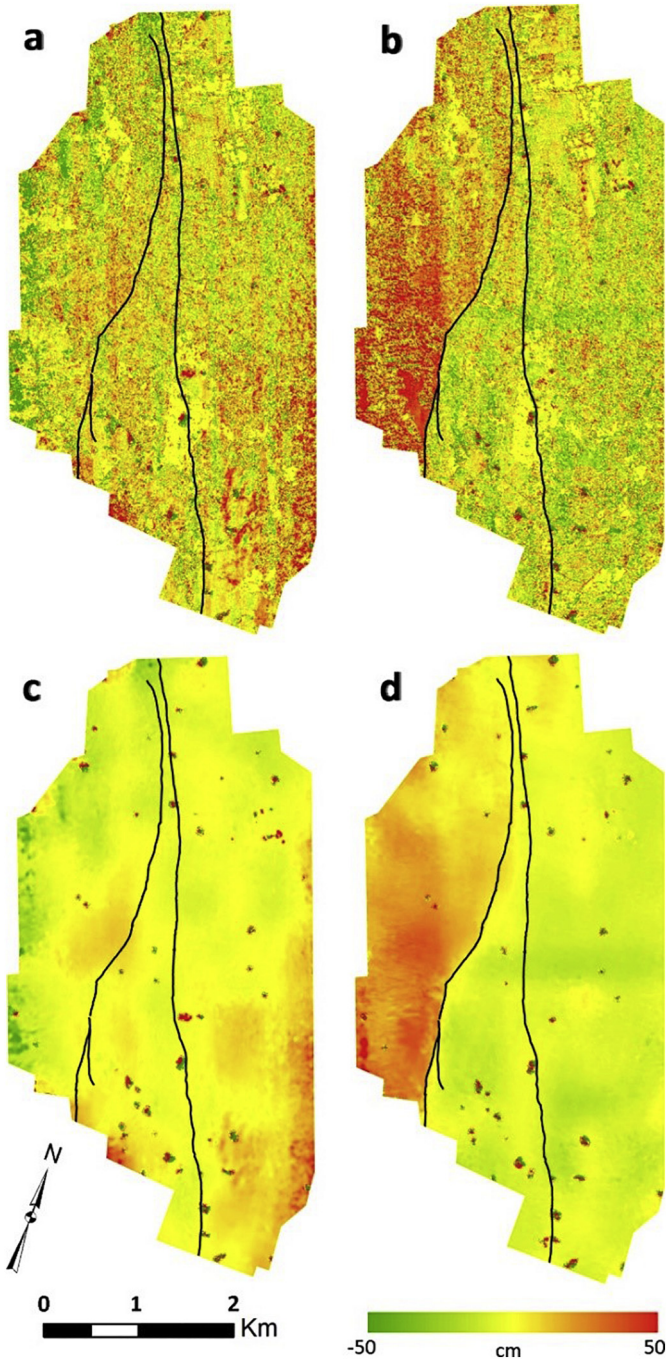

Fig. 5. Horizontal components of surface displacement in South Napa derived from laser intensity images using COSI-Corr along (a) east-west and (b) north-south directions; (c) and (d) were created filtering (a) and (b) using NL-Means. Figure originally from Ekhtari and Glennie (2017), used with permission.

case studies, the analysis focused on densely-vegetated sections of the surface ruptures. The results showed a smoothly varying, 3D displacement field from the Iwate-Miyagi rupture that indicated significant right-lateral slip along the fault with a component of dip-slip. These findings are in a close agreement with field observations and published focal mechanisms and fault models of the earthquake. Despite using a different post-event data collection, the horizontal components of ICP resemble those of Mukoyama (2011) that were obtained from PIV. Similarly, a smoothly-varying uplift/subsidence pattern along the Fukushima-Hamadori rupture was revealed by the vertical components of the ICP results (Fig. 6). The horizontal components, on the other hand, did not indicate any clear lateral motion along the rupture. While this behavior is expected for a steeply dipping, normal faulting event, the lack of a clear discontinuity along the rupture also suggests that horizontal component signal was lost to the noise (Nissen et al., 2014).

The surface rupture caused by the 2010 El Mayor – Cucapah, Mexico earthquake was the very first rupture with complete pre- and post-event ALS data. In an early study discussed above, Oskin et al. (2012) presented the initial estimates of vertical displacement but also highlighted significant systematic errors due to improper calibration of the pre-event data, which manifested as erroneous displacement estimates. Later on, Glennie et al. (2014) explicitly identified these systematic errors through the use of ICP. The initial ICP results revealed a significant periodic trend in the north-south displacement estimates along the rupture. In an effort to minimize these errors, Glennie et al. (2014) reprocessed the pre-event data and reevaluated the 3D displacement and rotation. The resulting improved ICP components revealed a significant right-lateral slip along with the dominant vertical displacement, which could not be measured using DoD.

Later on, Zhang et al. (2015) introduced an anisotropic-weighted ICP (A-ICP) algorithm and explored the use of a moving window to estimate surface deformation in greater detail. The proposed implementation was evaluated by estimating the known displacement in simulated data with synthetic fault ruptures as well as estimating the surface deformation caused by the 2010 El Mayor – Cucapah earthquake using pre- and post-event data. A-ICP has been shown to outperform standard ICP in estimating the synthetic displacement and even better estimates were obtained with the addition of the moving window technique. Despite unusually low point density in the pre-event data, the combined moving window A-ICP algorithm provided significantly smoother and more accurate displacement estimates than standard ICP.

Ekhtari and Glennie (2017) adopted the moving window ICP method and compared the estimates of horizontal displacement caused by the 2014 South Napa earthquake with those obtained from COSI-Corr using laser intensity images. It was shown that decimeter scale horizontal displacement could be resolved using both methods. The disparities between these methods were analyzed by differencing the estimation maps. COSI-Corr and moving window ICP have been found to demonstrate similar performance in estimating the horizontal displacement. However, COSI-Corr was much faster computationally. For a subset of the same study area, Lyda et al. (2016) employed standard ICP and compared its performance with PIV in estimating the horizontal displacement. While both methods provided distinctive displacement fields, the accuracy of ICP was significantly higher than that of PIV. Including geodetic markers (manmade structures) in ICP increased its performance even further.

In a recent study, Scott et al. (2018) calculated the 3D surface deformation caused by the 2016 Kumamoto, Japan earthquake by applying a windowed implementation of ICP to repeat ALS point clouds. The focus of the analysis was on the on- and off-fault coseismic surface deformation and strain fields, which, in turn, illustrate the behavior of the surface-rupturing earthquake at shallow depths. Displacement discontinuity measurements at several apertures (35 m, 100 m, and 1 km) indicated the presence of inelastic and spatially distributed off-fault deformation. This study demonstrated that repeat ALS data provide valuable information not only about the fault slip but also about off-fault displacement and coseismic strain field. Additionally, an empirical error metric, displacement correlation error, to evaluate the relative quality of ICP displacement is proposed. Unlike point-to-plane error, a metric to measure the quality of alignment between point clouds, the newly proposed metric measures the 3D displacement uncertainty. The displacement correlation error analysis of the ICP results indicated errors up to a few decimeters, which correlate with surface relief and land cover across the 50 m ICP window size.

As an alternative to ICP, Borsa and Minster (2012) presented the cross-correlation of point clouds which simultaneously compares topography and laser intensity between pre- and post-event data to

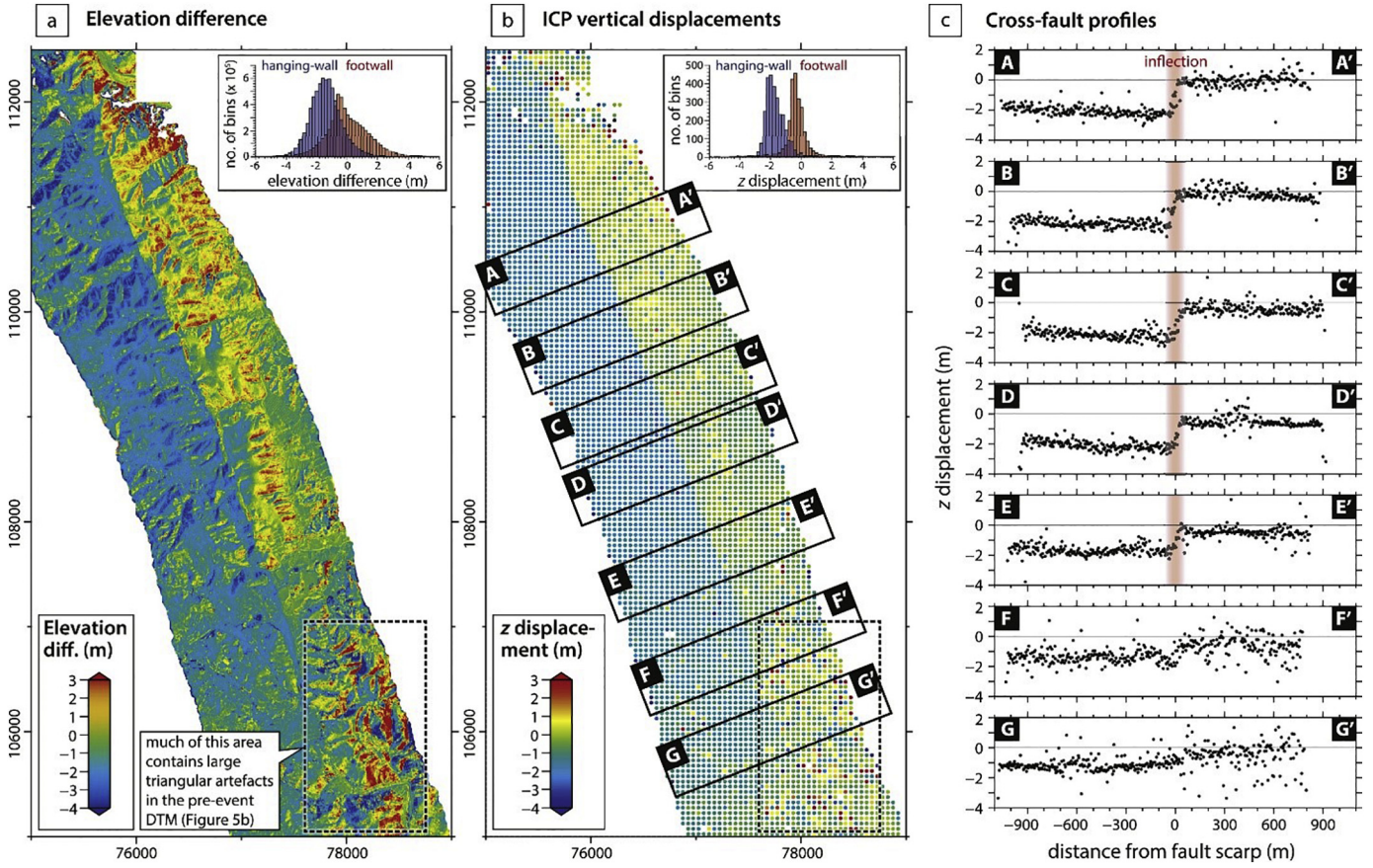

Fig. 6. (A) Change in elevation obtained through DoD and (B) vertical component of surface displacement obtained through ICP. (C) cross-fault swath profiles created from (B). Figure originally from Nissen et al. (2014), used with permission.

estimate 3D surface deformation rapidly. The post-event point clouds were obtained synthetically by deforming the pre-event data; the "B4" ALS survey of the San Andreas Fault (Bevis et al., 2005). The results indicated that the proposed method could recover the synthetically introduced deformation with an accuracy better than 20 cm horizontal and around 1 cm vertical.

3.3.3. Morphodynamics

Morphodynamics are defined as the changes to a landscape as a result of erosional and depositional processes by which distinct topographic features are formed. Repeat ALS data are frequently used to assess sediment budget, sediment transport, and spatial patterns of morphodynamics across large areas. Due to the extent of the studies evaluating morphodynamics across different landscapes (i.e., coastal and inland) and a wide range of environments, this topic has been subdivided into application-focused sections.

3.3.3.1. Coastal applications

3.3.3.1.1. Shore and near-shore. The use of repeat ALS products for evaluating morphodynamics in coastal landscapes have been demonstrated in numerous studies. Woolard and Colby (2002) used lidar-derived DEMs for spatial characterization and volumetric change estimation of the coastal dunes in Cape Hatteras, NC. This study also evaluated the effect of using DEMs with different spatial resolutions (1–20 m) on feature representation and volume change estimation. White and Wang (2003) investigated the spatial pattern of morphodynamics along oceanfront beaches of five barrier islands in North Carolina. The DoD results revealed that undisturbed beaches that were managed differently (i.e., undeveloped, developed, nourished) exhibited different net volume change. However, if the beaches were disturbed by consecutive storm events, the differences disappeared. Mitasova et al. (2004) investigated morphodynamics in the coastal landscapes of Jockey's Ridge State Park and Bald Head Island, NC using the DoD technique. The spatial pattern of erosion and deposition in the Jockey's Ridge sand dune field indicated a possible acceleration of the long-term erosion and migration process in recent years. Important aspects of beach evolution in Bald Head Island were also revealed: although the entire length of the beach retreated, the western section lost all nourished sand, whereas the eastern section exhibited significant volume increase. Young and Ashford (2006) evaluated seacliff and gully-beach sediment budget contributions to the Oceanside Littoral Cell, San Diego County, CA during a relatively dry period. The DoD results indicated substantial beach-sediment contribution from seacliff erosion and significantly lower gully beach-sediment contribution to the Oceanside Littoral Cell than was previously reported in the literature. Zhou and Xie (2009) studied the morphodynamics along Assateague Island National Seashore, VA and MD. The volumetric changes in the coastal landscape were evaluated in sections defined based on their historical changes and coastal conditions. The analyses of annual and four-year DoD grids indicated complex erosion-deposition cycles within the defined sections.

While DoD is a commonly used method in evaluating morphodynamics across coastal landscapes, a number of other methods have also been implemented (Brock et al., 2004; Mitasova et al., 2009, 2010; Richter et al., 2013a; Starek et al., 2012). Mitasova et al. (2009) proposed a *per-cell* statistics method to analyze ALS-derived DEM time-series in order to investigate spatial patterns of morphological change. For each DEM cell, multi-temporal, simple descriptive statistics (e.g., mean, median, standard deviation, etc.) or more complex relationships (e.g., parameters of linear regression) were calculated. Subsequently, a set of grids representing temporal trends in spatial patterns of morphological change were generated. The method was applied to Pea

Island Wildlife Refuge, a barrier island in NC, to investigate the evolution of beach and dune systems. A time-series analysis of 13 ALS data collections indicated that, in terms of elevation changes, the foredunes are the most dynamic feature in the area. The spatial pattern of morphodynamics suggested a trend toward inland sand transport and a significant wind contribution to sand transport. Mitasova et al. (2010) employed the *per-cell* statistics method to investigate decadal evolution of beach and dune systems on two barrier islands in the Outer Banks, NC. Similarly, foredunes were found to have the highest variation in elevation in both study areas. The results indicated that beaches and the ocean side of the dunes exhibited significant volume loss, whereas the landward side of the dunes exhibited a slight volume gain, a pattern consistent with barrier island transgression.

Richter et al. (2013a,b) monitored dune cliff erosion and beach-width change at the northern (Ellenbogen) and southern (Hörnum-Odde) spits of Sylt, Germany. A semi-automated dune-cliff breakline extraction method based on image filtering methods was presented. The results indicated spatiotemporally variable morphodynamics in both study areas. While dunes exhibit erosion only during winter due to storm surges, the beach width varies throughout the year due to highly dynamic shoreline. The effect of beach width on dune erosion was found to be dissimilar at the two study sites. Overall, the maximum dune cliff retreat was estimated to be 140 m at Hörnum-Odde and 70 m at Ellenbogen.

Cross-shore profile sampling of ALS-derived DEMs has also been used to characterize morphodynamics across coastal landscapes. Brock et al. (2004) proposed methods for calculating a set of laser metrics to assess the morphology and morphodynamics of barrier islands. Using these metrics, the coastal evolution along 10 km of the Northern Assateague Island National Seashore was analyzed. The morphology of the barrier island was defined based on static metrics as a set of attributed linear features based on the datum and longshore volume variation, whereas the morphodynamics were described based on change metrics calculated by differencing the static metrics. Most of the study area was found to be degradational with volume loss along both the bay and ocean shorelines. Of all the laser metrics obtained, the barrier island volume balance line (i.e., a combined linear-volumetric static metric) was found to be the single most important metric to provide information on the barrier dynamics. The analysis demonstrated that, through the use of laser metrics, even minor changes to barrier island morphology can be resolved. Starek et al. (2012) presented a framework for the probabilistic detection of morphologic metrics to assess short-term spatial patterns of coastal landscape evolution. The techniques were evaluated on a portion of St. Augustine Beach, FL. A total of nine morphologic metrics were parameterized from ALS-derived DEMs into several cross-shore profiles progressing alongshore, which were subsequently partitioned into erosional and depositional segments based on shoreline change over time. The potential of these metrics to identify zones of erosion and deposition was assessed. The results demonstrated that morphologic metrics indicative of spatial patterns of shoreline evolution can be detected and extracted systematically from repeat ALS data. However, the authors emphasized that, while promising results were obtained, the performance of the proposed technique is highly dependent upon the data, the physical characteristics of the site, and the coastal processes along the shorelines.

Studies concerning coastal morphodynamics have typically focused on beach-dune systems and rarely on the near-shore area. Tidal inlets and adjacent shorelines, however, exhibit significant changes in a relatively short amount of time as they are continuously modified by erosion-deposition processes and thus, monitoring morphologic evolution in these dynamic environments is of importance to coastal system management. In one such study, Levoy et al. (2013) investigated the formation and migration of long-crested transverse bars near a tidal inlet along the macrotidal west coast of Normandy, France on the basis of DoD. A large sediment platform in the tidal inlet was found to be the source of the sand for the transverse bars. Time-series analysis indicated a consistent northward migration of the bars with a mean rate of about 2 m per month. Monitoring the response of transverse bars to six consecutive tides under fair-weather conditions showed that strong spring tides are sufficient to maintain bar migration in the absence of waves. Expanding the work of Levoy et al. (2013), Montreuil et al. (2014) evaluated the spatial patterns of morphodynamics of the shoreline and ebb delta near a tidal inlet along the macrotidal west coast of Normandy, France. In addition to DoD, topographic profiles extracted from seven ALS data collections were analyzed. The results indicated a clear sand recirculation pattern in the tidal inlet. As opposed to commonly reported observations in wave-dominated macrotidal environments, the sediment transport pattern in the area did not suggest any inlet sediment by-passing. However, it was also noted that the influence of tidal channels on sand transport remains unclear.

3.3.3.1.2. Coastal lowland permafrost. Morphodynamics in coastal lowland permafrost landscapes are drawing increasing attention due to increased sediment release to the Arctic Ocean and mobilization of old organic carbon from these landscapes. Only a few studies, however, used repeat ALS data to characterize spatial patterns of coastal permafrost erosion and to estimate volumetric change over time (Jones et al., 2013; Obu et al., 2017). Jones et al. (2013) used repeat ALS data in DoD to detect morphologic changes associated with thermokarst and other thaw-related processes in the Beaufort Sea coastal plain of northern Alaska. Erosional features associated with thermo-erosional gullies and coastal, river, and lake bluffs indicated ice-rich permafrost degradation, which accounts for about half of the volume change over the study period in the area. The majority of the remaining volume change was found to be associated with the erosion of beach and spit deposits, riverine and deltaic flats, and sand dunes. Significant subsidence was observed in > 300 thermokarst pits, likely due to storm-surge flooding. Obu et al. (2017) investigated the magnitude and spatial patterns of short-term coastal morphodynamics in different landforms of the Yukon coastal plain and Herschel Island along the Canadian Beaufort Sea coast. The DoD results indicated spatially variable short-term movement and volume change along the permafrost coast. While the low-elevation coasts exhibit relatively uniform erosion, the high-elevation coasts, where mass-wasting is more prominent, exhibit more spatially varied erosion. Of all mass-wasting processes, retrogressive thaw slumping was found to be particularly important as it not only affects the slump location, decreasing erosion or even causing progradation, but also contributes to sediment input and accumulation at adjacent coasts due to significant sediment release.

3.3.3.1.3. Delta. While coastal wetlands represent some of the most dynamic landscapes, repeat ALS data have rarely been used to study spatiotemporal change in these landscapes. One such study assessed the elevation change and stability across the Wax Lake Delta (WLD), LA between 2009 and 2013 (Wagner et al., 2017). Multi-temporal ALS data were used to quantify the equilibrium elevation, subaerial slope adjustment, and volumetric changes to the delta. As opposed to DoD, vertical differencing of bare-earth point clouds was performed following the methodology outlined in Lague et al. (2013). However, the differenced point cloud was subsequently gridded in an effort to remove spatial clustering bias and present the data conveniently (Fig. 7). The analysis indicated that 83% of the delta surface exhibited net aggradation between 2009 and 2013, resulting in an elevation mode increase. Across the WLD, elevations around 0.56 m (above sea level) were found to be stable, suggesting the equilibrium elevation of the delta. The observed equilibrium elevation was then used to estimate the length of time required for the delta to approach stable elevation. The average equilibrium time for the system was found to be 16 years.

3.3.3.1.4. Response to extreme events. Extreme storm events play an important role in morphodynamics of coastal landscapes; thus, evaluating the changes induced by these events is of importance. Meredith et al. (1999) studied hurricane-induced morphodynamics

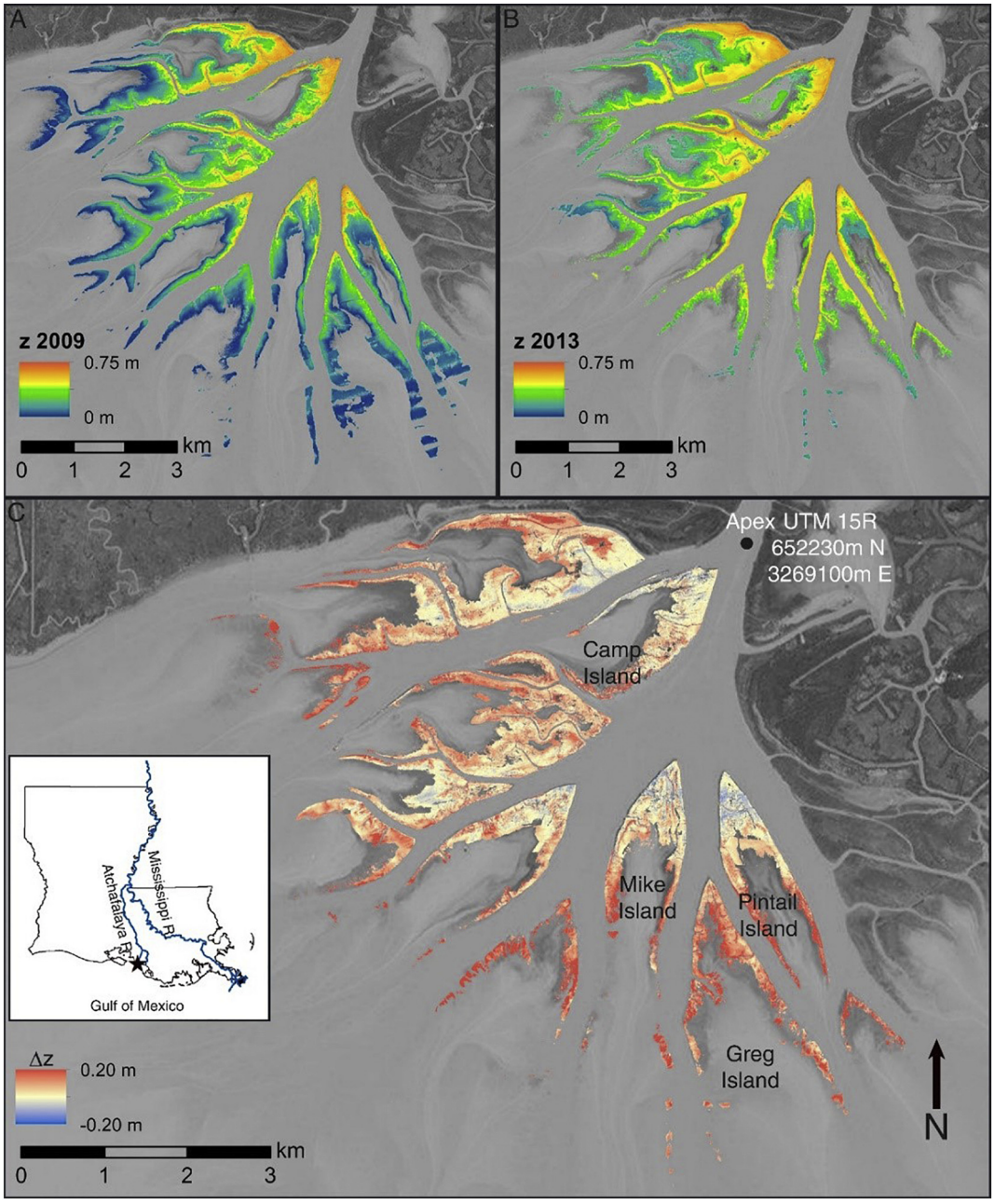

Fig. 7. Wax Lake Delta elevation in (A) 2009 and (B) 2013, and (C) the change in elevation over the four-year study period. Figure originally from Wagner et al. (2017), used with permission.

along the entire North Carolina coastline using ALS data collected in 1997 and again, immediately after hurricane Bonnie, in 1998. The volumetric change in beach sand due to deposition and erosion caused by the hurricane was estimated using lidar-derived DEMs. The results showed a spatial pattern of sediment loss and gain along the NC coastline in response to this major storm event. Sherman et al. (2013) investigated the impacts of hurricane Ike on the sandy beaches of the Bolivar Peninsula, TX with a particular focus on the scour features formed by the ebb flow of the storm surge. The DoD grids were created from five sequential ALS data collections acquired in 2006, 2008 (in September immediately after the hurricane and December), and 2009 (in February and April). The morphologic changes were then identified and quantified through the implementation of the object-oriented method outlined in Liu et al. (2010). The results showed the development of five distinct types of scour features along the beaches of the Bolivar Peninsula induced by the hurricane. The identified scour types were not uniformly distributed alongshore but rather clustered depending upon the ebb flow environment. It was also noted that many of the identified features persisted for months after the hurricane. The total sediment loss caused by the hurricane was estimated to be $> 100\,m^3$ per meter of the investigated portion of the beach, which is larger than previously reported values. The response of sandy and gravel beaches of southwest England to extreme storms during the 2013–2014 winter was studied in 157 beach sections along the coast of Somerset, Devon, Cornwall, and Dorset counties on the basis of net volumetric change and the newly introduced longshore variation index (LVI) derived from DoD grids (Burvingt et al., 2017). Based on the analysis, four distinct types of beach responses were identified. The spatial distribution of beaches of different types was found to be coherent at a regional scale with several outliers disrupting this coherence at a local scale. Pye and Blott (2016) used cross-shore profiles along the Sefton Coast, northwest England to assess the impact

of the stormy 2013–14 winter on coastal morphodynamics in the context of longer term trends using ALS data acquired in 1999, 2013, and 2014. Changes in the dune toe position along the profiles and the sediment volume in the upper beach and frontal dunes within the defined sections were quantified. Subsequently, short-term changes (2013–2014) were compared to relatively longer term changes (1999–2013 and 1999–2014). Overall, short-term sediment budget estimations indicated a net loss of sediment from both beach and frontal dune systems while some parts of the beach to the south of the study area exhibited sediment gain, suggesting southward sediment transport. Likewise, long-term sediment budget estimations indicated net sediment loss in the central part of the study area. However, the upper beach and dune systems to the south and north exhibit net sediment gain over the study period. The findings of this study indicated that, while major storm events impact short-term morphodynamics significantly, their impact on long-term coastal evolution can be limited.

3.3.3.2. Inland applications

3.3.3.2.1. Fluvial. Despite its influence on morphodynamics and sediment budget, accurately estimating sediment transport in steep mountain streams remains a challenge. Anderson and Pitlick (2014) used repeat ALS data to quantify fluvial sediment transport along Tahoma Creek, WA (Fig. 8). The amount of sediment transported through a given cell was estimated by summing the DoD-derived volumetric change upstream of that cell on the basis of morphologic budgeting. The results suggested that the sediment transport between 2002 and 2008 was dominated by the 2006 flood. The ALS-based sediment budget estimates suggested that unconsolidated glacial sediment were mobilized from the upper basin, likely by debris flows. The sediment mobilized between 2008 and 2012 was an order of magnitude less than the previous (2002–2008) period. In both time periods, however, more than half of the mobilized sediment was transported past the downstream extent of the study area, while the most of the remaining sediment was deposited along the upper half of the creek.

Cavalli et al. (2017) used repeat ALS data to assess the morphodynamics in two adjacent steep mountain basins in the eastern Alps (Gadria and Strimm) with contrasting morphology and different types of sediment transport processes. The results indicated that, although both the Gadria and Strimm catchments exhibited net volume loss, the morphodynamic spatial patterns were significantly different. In the former, erosion occurred predominantly toward the upper portion of hillslopes and gullies; whereas in the latter, most of the erosion occurred along the lowermost reach of the main channel. The DoD analysis facilitated investigation of the relationship between morphodynamics and geomorphometric parameters (e.g., slope, contributing area, curvature). It was found that erosion in both catchments occurred primarily across persistently concave (up) surfaces or those transformed into concave surfaces; whereas deposition mostly occurred across convex surfaces. Volume changes estimated from the DoD grid were compared to in-situ measurements collected after specific events between July 2005 and June 2011. Overall, DoD-derived estimates were found to be larger than field observations in all cases except for the deposition estimates in Strimm basin.

3.3.3.2.2. Eolian. In contrast to numerous successful applications in coastal landscapes, the application of multi-temporal ALS to assess dune migration and erosion in eolian landscapes has been limited (Dong, 2015; Reitz et al., 2010). Lidar-derived DEMs were used in DoD to evaluate a predictive model for the downwind transition of barchan dunes into more stabilized parabolic dunes in the White Sand Dune Field, NM (Reitz et al., 2010). The model-predicted transition pattern was found to correspond well with the observed spatial relationship. Confirming the model-predicted threshold, the results showed that the barchan-parabolic transition occurs when the ratio between erosion and deposition rates across the dune surface decrease below half of the vegetation growth rate. Dong (2015) proposed the Pairs of Source and Target Points method for automated measurement of dune migration direction and rate. The method was evaluated using multi-temporal ALS data from the White Sands Dune Field. The centerlines of dune slip

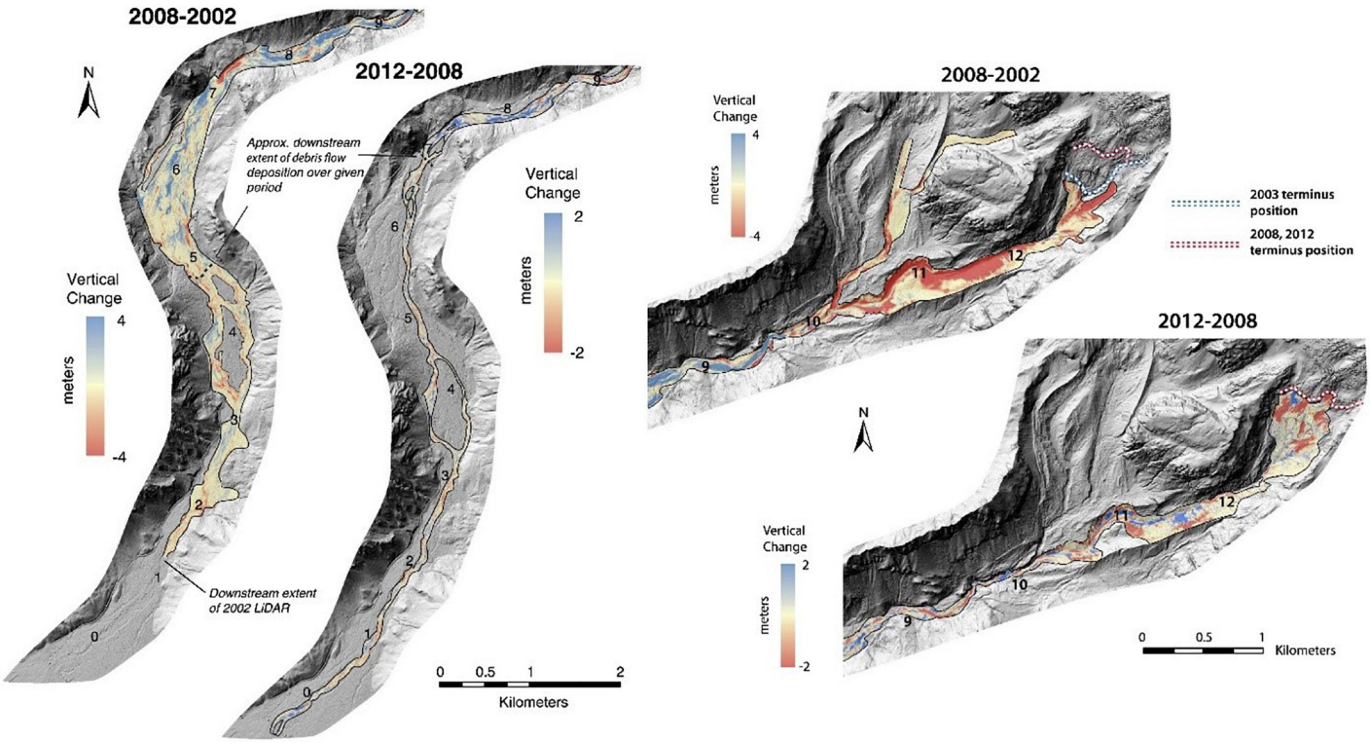

Fig. 8. ALS-derived DoDs showing the vertical change in (A) the lower and (B) the upper basins of Tahoma Creek. Figures originally from Anderson and Pitlick (2014), used with permission.

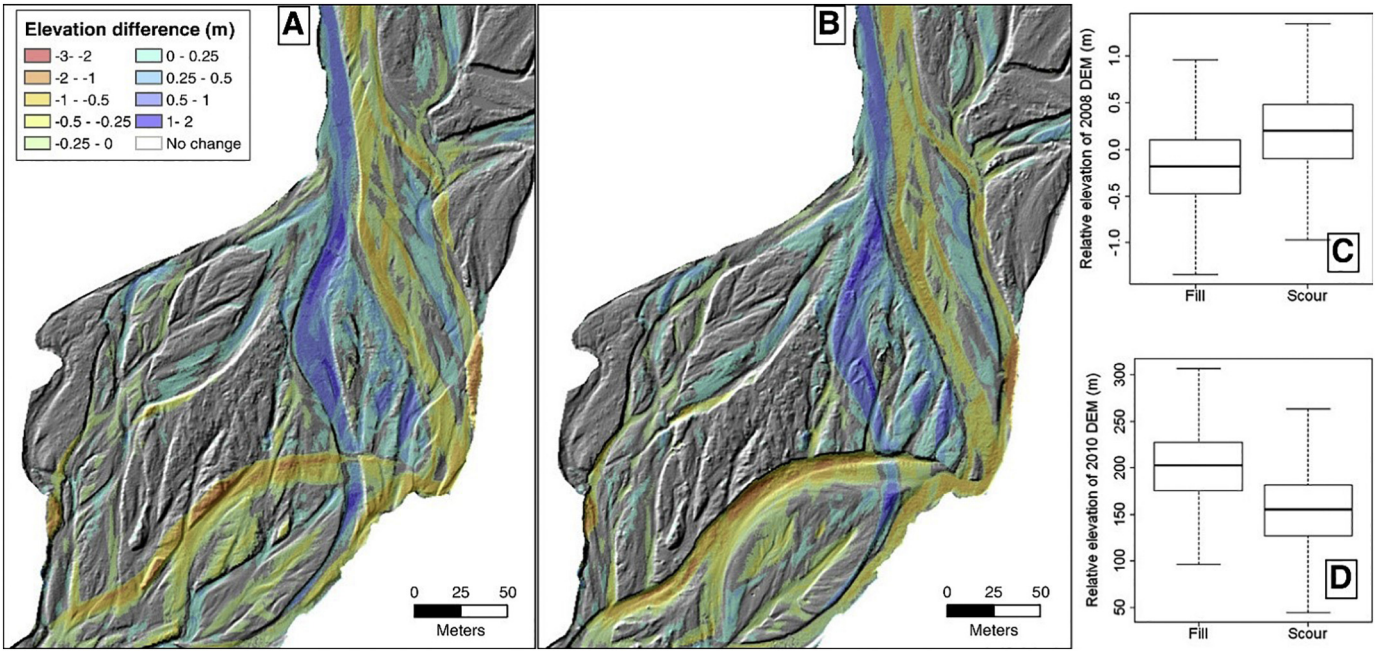

Fig. 9. The DoD grid draped over shaded relief views of (A) 2008 and (B) 2010 ALS-derived DEMs. Distribution of relative elevations for fill and scour pixels in (C) 2008 and (D) 2010. Figure originally from Lallias-Tacon et al. (2014), used with permission.

faces in different epochs of ALS-derived DEMs are extracted as the source and target lines based on a range of slope angles. Random points along the target line were selected and paired with corresponding points on the source line. Source direction and migration distance were estimated using the paired points. The overall spatial pattern of dune migration was then evaluated on a surface grid that was interpolated using migration rate estimates. In this case study, the majority of the extracted target points had a source direction approximately parallel to prevailing winds (225°–285°) and suggest migration rates between 4 and 7 m/yr with an average rate of 5.56 m/yr. The spatial distribution of migration rates suggested that deviations in source direction of up to 30° from the prevailing wind direction do not have a significant effect on migration rates. It was also noted that the Pairs of Source and Target Points method is not exclusive to sand dune migration and can potentially be modified and implemented in many other morphologic change detection applications.

3.3.3.2.3. Glacial. While studying morphodynamics in glacial landscapes using repeat ALS has been limited, a few studies have taken advantage of these data (Irvine-Fynn et al., 2011; Sailer et al., 2012). Irvine-Fynn et al. (2011) quantified short-term morphodynamics and sediment redistribution in the forefield of Midtre Lovénbreen, Svalbard using ALS data coupled with in-situ measurements. The DoD analysis revealed two primary areas of sediment reworking: active fluvial incision of proglacial streams and lateral moraine downwasting both of similar magnitudes (~2 m). The ALS-derived sediment loss did not correspond well with the observed sediment load in fluvial systems, suggesting significant quantities of buried ice among the eroded volume. One other study in the Swiss Alps utilized 18 ALS data collections to characterize rock falls, erosion, fluvial erosion, and topographic changes (Sailer et al., 2012). Annual and multi-annual elevation differences were calculated using an Approximate Nearest Neighborhood (ANN) method. The ANN works similar to DoD, except vertical differences are calculated between two closest points within a search radius. The scope of the investigation created a far more comprehensive picture of the interactions between receding or disappearing glaciers and the terrain their departure leaves behind. The greatest changes were, in fact, noted in regions that had previously been glaciated as these areas responded rapidly to increased water flow, ground thaw, and the loss of stabilizing glacial ice. Overall, a mean decrease in elevation across the study site was recorded but, beyond that, the changing face of a very dynamic region of the cryosphere was captured by the biannual ALS collections.

3.3.3.2.4. Response to extreme events. Infrequent, large magnitude events (e.g., floods, wildfires, rainstorms, etc.) can cause abrupt changes inland and thus, are crucial for better understanding and monitoring landscape evolution. Croke et al. (2013) assessed the basin scale spatial patterns of erosion, deposition, and net volumetric change in the Lockyer Creek catchment of SE Queensland as a result of catastrophic flood event in 2011. A one-dimensional flow hydraulic model, HEC-RAS, coupled with the DoD grid, was used to delineate five major landforms (i.e., inner-channel bed, inner-channel bank, within-channel bench, macro-channel bank, and floodplain) of the fluvial morphology. The distribution of elevation changes suggested that a large portion of the 100 km^2 study area exhibited relatively low magnitude change with a mean elevation change of 0.04 m. The ability to evaluate different landforms separately revealed a spatial pattern of morphodynamics within and between these landforms. The results indicated that only the within-channel benches and macro-channels exhibit net erosion, whereas the inner-channel bed and banks exhibit net deposition. These findings indicated sediment redistribution to be the dominant process in the investigated area.

Lallias-Tacon et al. (2014) used repeat ALS data to evaluate morphodynamics in a segment of a gravel-bed river channel near Digne-les-Bains, France following a 14-year return period flood. Prior to the DEM creation, the multi-temporal ALS data were aligned using ICP based on stable surface features. To obtain the submerged topography of the river channel, the water depths measured in-situ were subtracted from the water surface elevations along the channel, which was manually delineated on point density maps as outlined in Legleiter (2012). The morphologic sediment budget was computed sequentially after each processing step to assess their respective influence. The final DoD grid clearly highlighted a lateral shift of the main and secondary channels over the study period (Fig. 9). A large portion of the active channel, except for some vegetated islands, had been reworked. Due to channel avulsion in response to the flood, the braided channel pattern was found to be highly disturbed.

Moretto et al. (2014) assessed the short-term morphodynamics along three successive sub-reaches of the Brenta River, Italy caused by

two major flood events in November and December of 2010. In an attempt to describe the changes in fluvial morphology associated with the flood events adequately, hybrid digital elevation models (hDEMs) were created by merging ALS data (dry areas) with color bathymetry and dGPS (wet areas) surveys. While all three sub-reaches exhibit net sediment loss, the volumes of sediment lost and gained were found to be converging downstream. In support of this, the lowermost sub-reach could be divided into an erosion-dominant upper portion and a deposition-dominant lower portion. The DoD analysis suggested that erosion in the two uppermost sub-reaches consistently occurred along the main channels and that continuous erosion and deposition along the main channel led to channel migration in the middle sub-reach. The different spatial pattern of erosion and deposition between the analyzed sub-reaches was attributed to their diverse morphologic characteristics and differential sediment supply from upstream.

Repeat ALS data collections were used to evaluate morphodynamics and estimate sediment budget in Blue Earth County, MN where the occurrence of an extreme flood in 2010 caused landscape-scale changes (Schaffrath et al., 2015). In addition, the effect of different DoD uncertainty assessment approaches on a landscape-scale estimation of sediment budget was evaluated. Consequently, volume change estimates for Blue Earth County were made using three approaches: (i) no thresholding, (ii) spatially uniform thresholding, and (iii) spatially variable thresholding. Although all three approaches indicated net sediment loss, the volume estimates were not similar. Estimates of erosion and deposition obtained with no thresholding were significantly higher than those obtained from the two thresholding approaches. The net volumetric change, however, was grossly underestimated with the no thresholding approach. In comparing the spatial patterns of morphodynamics highlighted by these different uncertainty models to field observations, results from the spatially variable model were found to be in a closer agreement with in-situ observations. Applying the spatially uniform uncertainty threshold was shown to produce inaccurate volume estimates; while real change along the main channel was eliminated, erroneous change along the ravine slopes was incorrectly detected.

Wicherski et al. (2017) used repeat ALS data coupled with in-situ measurements to investigate morphodynamics along a floodplain of Fourmille Creek, CO, which was devastated by a severe flood event in 2013 that followed a wildfire in 2010. The DoD highlighted areas of deposition flanked by areas of erosion, sediment bypass, or mixed erosion/deposition. The entire floodplain, however, was found to exhibit net erosion and was lowered during the flood event by around 0.25 m. Comparisons with in-situ measurements revealed that net erosion estimates derived from DoD analysis were typically higher. The findings of this study demonstrated that long-duration flood events in mountain streams can account for a large fraction of total sediment transport.

Pelletier and Orem (2014) investigated the morphodynamics and sediment yield associated with the 2011 Las Conchas wildfire and subsequent rainstorm events. An automated method for computing the net sediment volume exported through each pixel within the drainage basin was proposed and evaluated. In an attempt to minimize the effect of uncertainties in the data, a 0.3 m threshold, chosen based on the stated accuracy of the ALS data, was applied to the DoD grid. Sediment volume was found to be proportional to the upstream contributing area, whereas the average sediment yield (i.e. volume per unit contributing area) was a power-law function of the average terrain slope and soil burn severity class. Later on, multi-temporal ALS and TLS surveys were used following the Las Conchas fire, NM, to monitor the post-fire changes in erosion rates within two small watersheds (Orem and Pelletier, 2015). Erosion rates in both study areas peaked after the fire and then dropped off; however, local factors led to different drop off responses in each area. Despite these variable responses, both study areas took approximately one year to return to pre-fire erosion rates, suggesting that the regional vegetation had sufficiently recovered within a year to once again become the dominant forcing for local erosion rates.

Anderson et al. (2015) investigated the morphodynamics in the Front Range of Colorado associated with a massive storm event. Using repeat ALS data collected in 2010 and shortly after the storm in 2013, a total of hundred and twenty mass movements triggered by the storm were identified and the net volume changes in these movements were estimated. The DoD results indicated that while the lowering depths calculated as averages for basins that contained mass movements ranged between 0.4 cm and 0.5 m, the area weighted averages for crystalline and sedimentary regions were found to be 0.16 cm and 0.21 cm, respectively. Comparing the basin-averaged lowering depths to the published long-term erosion rates suggested that the estimated exhumation caused by these mass movements corresponds to hundreds to thousands years of weathering products.

3.3.4. Landslides

Repeat ALS collections are frequently used to quickly and safely detect and characterize mass wasting events (Bull et al., 2010; Burns et al., 2010; Corsini et al., 2009; DeLong et al., 2012). The relatively fine resolution offered by ALS can be used to isolate individual patches of movement that are part of a larger landslide event when three or more ALS collections are available. In heavily forested areas, ALS can be used to locate landslide signals that might otherwise be difficult to find (Burns et al., 2010).

Identifying landslides, particularly in forested regions with multiple, smaller landslides, is challenging. One study conducted in Oregon found that using repeat ALS to detect events improved detection rates dramatically (Burns et al., 2010). ALS surveys were conducted in two separate seasons to capture the forested region both with and without foliage. The survey results were translated into DEMs and compared to find landslides and quantify the amount of material lost to these events. Nearly thirteen times the number of previously detected landslides were located in the study region using ALS. However, the study reported that thresholds needed to be applied to the difference between the DEMs in order to remove the effects of seasonal variations and to reduce the number of erroneous landslide identifications. The inherent differences between the foliated and unfoliated ALS data also caused problems when calculating the total material loss in the study area due to landslides alone. Consequently, Burns et al. (2010) recommended that ALS data should be collected in unfoliated conditions whenever possible.

Beyond using DoD created from ALS to identify landslides, it is also a commonly used technique to track landslide progress and quantify the volume of material displaced in landslides. This technique was used in Italy to track landslide progress in order to protect populations living in the affected region (Corsini et al., 2009). The results of differencing ALS-based DEMs in this study showed an order of magnitude less bias than photogrammetric methods. However, the largest source of error in the study came from the interpolation necessary to model the bed structure below the landslide, which was not independently surveyed before the start of the event. A typhoon in Taiwan in 2009 induced widespread landslide activity, which would have been difficult, if not impossible, to quantify using traditional field methods (Tseng et al., 2013). In one part of the study area, over 75″ of rainfall was recorded over a 72 h time period. Over three hundred landslides and their initiating crown areas were mapping using the DoD method. Additionally, a subsequent study examined the ongoing erosional effects following the landslide events in Taiwan and showed that the landslides altered the evolution of the valleys they occurred in, when compared to valleys in the same region that did not experience landslides during the typhoon (Tseng et al., 2015). A study conducted in Poland paired the DoD approach with a machine learning algorithm designed to automatically detect landslides (Pawłuszek and Borkowski, 2017). Numerous characteristics were tested to refine the machine learning approach and each is documented in the original literature. Relief, offset, roughness,

elevation, slope, and aspect were the descriptive variables determined to have the most success in distinguishing landslides from the surrounding terrain; however, the final automated product still included misidentified terrain when compared to known landslide surfaces in the region.

Landslides following an extreme rain event in Matata, New Zealand, in 2005, were investigated using the DoD method, built on ALS data (Bull et al., 2010). Identifying regions of greatest material loss and gain was used to investigate landslide pathways. Landslide volumes attained from the DoD method were found to be similar to those derived from field measurements. However, post-event remediation work had already begun by the time that the second ALS flight was completed and so not all of the landslide pathways could be cleanly captured as some of the landslide remnants had been already altered. Erosion rates at an ongoing landslide at Mill Gulch, CA, have been measured using DoD from repeat ALS collections in 2003 and 2007 (DeLong et al., 2012). Rather than working around vegetation issues, the ALS data was first post-processed to only show bare-earth. The volume of displaced material and the average, catchment-wide erosion rates were then calculated based on the bare-earth DEMs. The ALS derived erosion rates were slightly higher than those calculated from cosmogenic radionuclide dating within the catchment but both agreed within an order of magnitude. Varying rates of erosion were noted around the catchment using the DoD product, which represented an important precursor to using repeat ALS data to derive non-uniform flow fields for mass wasting events.

Four ALS surveys were conducted of a landslide in Montaguto, Italy, and the product DEMs were used in a traditional DoD analysis to determine erosion and accretion rates as well as to identify landslide structures, such as cracks, folds, ridges, and grooves (Ventura et al., 2011). Particular emphasis was put on defining the landslide extent in each ALS data set and average velocities for both the crown and toe of the landslide were developed by pairing the boundary data with longitudinal cross sections in both regions (Fig. 10). Repeat ALS data of the Valoria earthflow in Italy was taken a step further and was actually used, after being rasterized, to determine the variable flow field throughout and across the periodically active flow (Daehne and Corsini, 2013). The technique they used, digital image correlation, is reliant on certain features being preserved even as they move. In the rapidly, but periodically, mobile Valoria earthflow, few features met the necessary criteria but the study found that some feature characteristics, such as slope gradient, were maintained from one activation to the next. The authors do note that velocities determined in this way depict trends, differentiating different flow regimes, rather than precise values. A more traditional DoD analysis to calculate loss and gain of material in different parts of the earthflow was also conducted. Three ALS surveys in 2003, 2006, and 2007, as well as annual TLS surveys, were used to capture the motion of a landslide in Doren, Austria (Ghuffar et al., 2013). The angle flow algorithm, more commonly used in computer science than Earth science, was used to map flow velocities. The technique pairs feature mapping with constraints on flow motion, which were not known a priori in this study and were built from a coarse to fine resolution assessment of varying DEM grid sizes. The results of this method were compared to motion of reflectors in the landslide and good agreement was found at nearly all of the reflector points, barring a few outliers.

ALS data, orthophotographs, and field data were all used to assess the effect of land cover on a forested and mountainous region of Austria (Schmaltz et al., 2017). Land cover type, broken into three categories – conifer, deciduous, and mixed, was considered in terms of both vegetation density and age. Despite the many variables considered in the analysis, forest cover, regardless of type or age, had the most significant effect on landslide susceptibility, with less vegetated regions experiencing more landslides than more vegetated regions. In a recently unglaciated region of Austria, multi-temporal ALS and TLS surveys were taken from 2006 to 2014 to monitor geomorphic changes to the receding glacier and the rapidly changing, freshly exposed surroundings (Vehling et al., 2017). Stability was maintained in unglaciated terrain for some time following its exposure as the ground itself remained frozen. However, as increasing amounts of meltwater were produced, the unglaciated terrain was observed to lose stability and both rock flows and rock slides increased in energy and frequency.

Building on the routine use of DoD methods to ascertain standard landslide parameters, Mora and Toth (2014) used this technique to assess the landslide susceptibility of an area near Zanesville, OH. The DoD results were used to isolate areas experiencing a high level of topographic change and, when paired with topographic information such as slope, landslide susceptible regions were identified. However, the results of the study were not compared to actual landslide data in the region after the fact, leaving the method somewhat untested.

4. Discussions and outlook

Connecting forest ecosystem processes or extreme events to carbon fluxes, AGB dynamics plays an important role in predictive analytics and management of terrestrial carbon (Hudak et al., 2012). With increasing availability, increasing numbers of studies taking advantage of repeat ALS data collections for estimating changes in AGB over time have appeared in the literature. Furthermore, successful use of multitemporal ALS in biosphere is opening new opportunities in critical zone research. Providing the unique opportunity to measure ecologic, geomorphologic, and hydrologic properties, repeat ALS data allow for the monitoring of change in the geosphere, hydrosphere, and biosphere simultaneously advancing the state of critical zone science (Harpold et al., 2015). While multi-temporal ALS allows for modeling AGB change, there are some uncertainties associated with the analyses. Two approaches, i.e., direct and indirect, have been implemented in modeling AGB change using repeat ALS data. The number of studies that implemented the indirect modeling approach are relatively higher than that of the direct approach but it is still unclear whether one approach is superior to the other. While a few studies have sought to evaluate the accuracies of the direct and indirect approaches in estimating AGB change, the results are not conclusive due to the limited number of studies and a consensus has yet to be built. To date, the validation of AGB estimates and the accuracy assessment of change detection have been commonly performed by comparing the lidar-derived estimates with in-situ estimates. A few studies also used TLS-derived estimates (e.g., Greaves et al., 2017; Li et al., 2015) for calibration and evaluation of ALS-derived AGB estimates. Initial results suggest that TLS can potentially provide ground-truth for calibrating ALS-derived AGB estimates. Nevertheless, both studies emphasized the need for high-quality in-situ data to establish the initial relationship between in-situ and TLS-derived estimates. Increasing complexity of the architecture of an ecosystem can lead to uncertainties in both in-situ and laser measurements. A rigorous assessment of uncertainties in individual data collections and accounting for them in AGB change detection analyses is not trivial and thus, subject of continuous research.

Far from using similar techniques to measure similar metrics, the wildfire community has used temporal ALS data to gauge fire severity and recovery time based on variable burn rates between different tree types and tree stress conditions, distance between tree canopies pre- and post-fire, and rates of tree fall. One of the key challenges to using ALS to study wildfires is the necessity for pre-event data, which can be hard to justify since wildfire hazards can rarely be accurately predicted. However, the forestry community uses ALS data extensively, providing a potential wealth of pre-fire data. Improving data resolution through the reduction of error and automating the detection of individual trees in ALS data are two avenues that would be beneficial across the spectrum of wildfire approaches seen in the current research. Additionally, no wildfire studies to date have taken advantage of multispectral lidar (e.g., Fernandez-Diaz et al., 2016), despite the clear benefits of paring traditional ALS data with Landsat spectral data. While multispectral

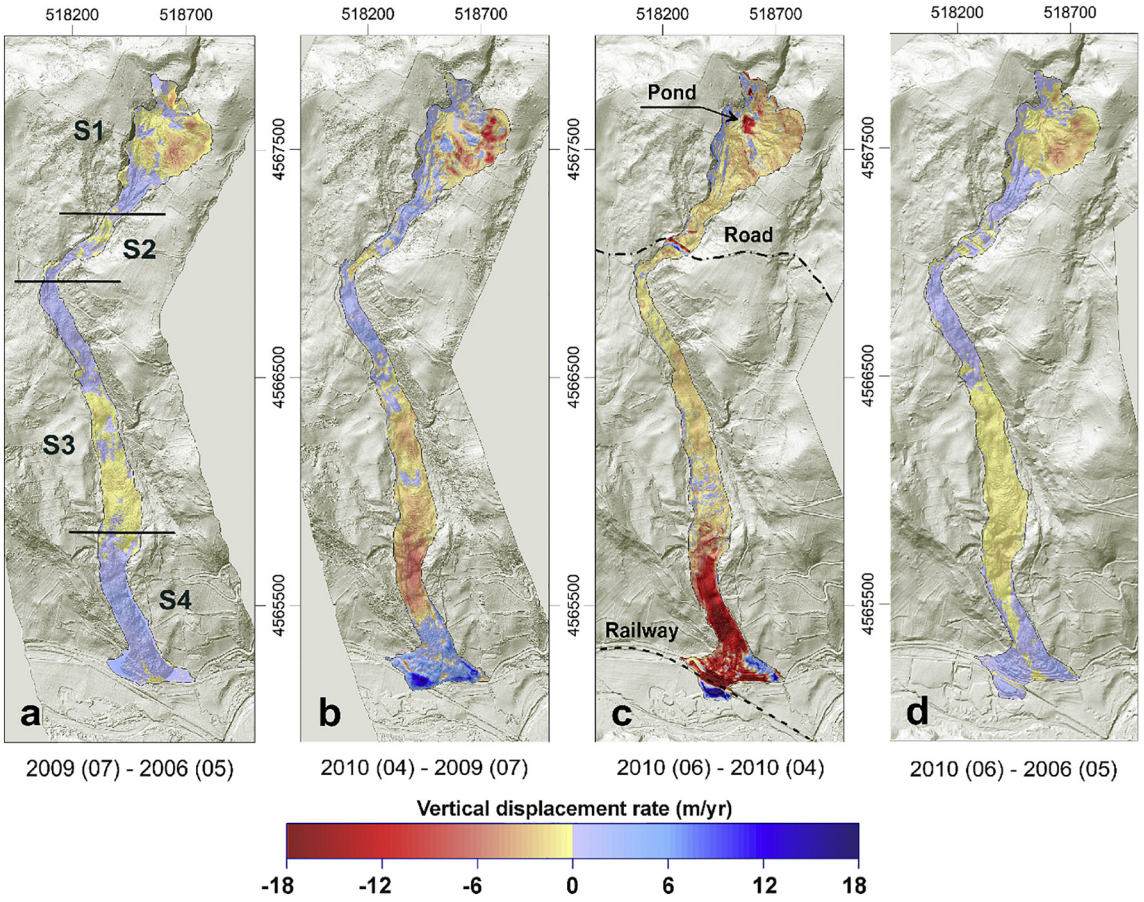

Fig. 10. The vertical displacement in the Montaguto landslide for four different epochs. Figure originally from Ventura et al. (2011), used with permission.

lidar data is unlikely to replace Landsat data, it may provide complementary information or be useful to fill in gaps where Landsat data is either unavailable or does not have high enough resolution.

Since the polar regions and high mountainous terrain of the cryosphere is typically difficult and hazardous, ALS offers key advantages, whether studying glaciers or snow accumulation and melt. ALS provides a significantly higher resolution than satellite data and can cover otherwise difficult to access areas more easily than ground-based measurement techniques. While this is generally applicable to other sub-disciplines as well, the short field season at the poles and in high elevation environments, coupled with the freezing temperatures, makes this especially impactful in the cryosphere. The most novel research in cryosphere science is to utilize lidar data properties beyond elevation, such as pulse return intensity. In an early study, ALS intensity data from the Swiss Alps was used to classify different types of terrain and evaluate change over time (Fritzmann et al., 2011). The ALS instrument used for the study operated at a single wavelength of 1064 μm and the results of the ALS intensity classification were compared to those from a classification of RGB orthophotographs. With increasing availability of operational multispectral lidar systems, pulse return intensity from additional wavelengths will likely to be more extensively used in cryosphere studies to classify surface feature and spatiotemporal change. A pilot study using multispectral ALS in Antarctica has demonstrated that pulse return intensity in different ALS wavelengths can be used to automate the differentiation of ground cover types including snow, ice, and bare earth (Okyay et al., 2018). Continued research in this direction will resolve changes to the cryosphere beyond those we are currently able to monitor and will inform our understanding of how cryosphere environments are changing in a greater level of detail. Another emergent application of repeat ALS to cryosphere science is estimating snow water equivalent (SWE) from lidar-derived snow depths. As it plays a critical role in controlling the volume and timing of snowmelt run-off, SWE is an important component of water resource management. The spatial variability in SWE is controlled by snow depth and snow density. While repeat ALS data have proven successful to estimate the snow depth across large spatial extents (Deems et al., 2013), coupling snow depth to SWE still remains a challenge. In order to address the knowledge gap in measuring spatial distribution of SWE, projects such as NASA Airborne Snow Observatory (ASO) and NASA SnowEx have been initiated.

Though ALS is often ideal for quantifying changes to remote environments, volcanoes present an unusually challenging environment for the collection and use of ALS data. Hazards at active volcanoes, including turbulent plumes even during less spectacular eruptions, high heat, and ash emissions, can complicate or preclude data collection. In addition, the steep slopes of many volcanoes increase the error inherent in ALS data. Resultantly, most of the repeat ALS surveys of volcanoes compare eruptive products in quiescent periods. However, during events like the 2018 fissure eruption at Kīlauea, HI, ALS has the potential to be immediately useful in an active and ongoing eruption (USGS, 2018a,b). Effusive eruptions, like those commonplace to Kīlauea, can be mapped safely by ALS with careful preplanning and ALS data can provide important, up to date information about lava flow rate and extent. A novel application of repeat ALS to volcanology is monitoring surface deformation caused by volcanic activity. A pilot study investigated the use of temporally spaced ALS data collections for detecting spatially distributed surface deformation around Yellowstone Caldera (Fernandez Diaz et al., 2018). Repeat ALS has the potential to bridge the gap between GPS and InSAR by detecting surface deformation more frequently across large spatial extents. However, subtle surface deformation signals pose specific challenges to data registration and accurate change estimation, particularly for noisy data collections.

Error propagation and uncertainty analysis is a requirement in these cases in order to be able to effectively separate signal from noise. However, to date, the propagation of uncertainty into final point cloud differences has received only limited attention (e.g., Hartzell et al., 2015; Wheaton et al., 2010).

Measuring surface deformation caused by earthquakes is important to determine the fault rupture geometry and to understand the mechanics of the earthquake. The expanded use of repeat ALS in measuring near-field surface deformation has the potential to bridge the observational gap between in-situ slip measurements and far-field deformation measurements from satellite data. To date, a wide variety of methods have been adopted to quantify surface deformation using repeat ALS data. In fact, among the multi-temporal ALS applications in Earth sciences, surface deformation studies are the most methodologically diversified. However, neither of these methods exploit the full potential of ALS for detecting surface deformation since they either assume rigid-body transformation (e.g., ICP and cross-correlation of point clouds) or are not 3D by nature (e.g., DoD, COSI-Corr, and PIV). Therefore, measuring non-rigid and fully 3D surface deformation remains a challenge. Assessment of distributed inelastic deformation that occurs adjacent to faults is of importance as it allows understanding of near-field and off-fault deformation patterns as demonstrated in Milliner et al. (2015, 2016) using image correlation. Although Scott et al. (2018) demonstrated the use of repeat ALS data for evaluating spatially distributed inelastic off-fault deformation and coseismic strain field comparing discrete displacement discontinuity measurements, the analysis is inherently limited by rigid-body assumption of ICP. Methods that track individual features in the point cloud (DeLong et al., 2015; Kusari et al., 2019), analogous to the use of persistent scatterers using InSAR (Hooper et al., 2004), show promise for providing spatially distributed estimates of deformation without assuming rigid body motion.

DoD has been, by far, the most commonly used method for evaluating morphodynamics in ALS change detection studies across different landscapes. With the expanding use of DoD for estimating volumetric change caused by erosion-deposition processes, the awareness of the need to assess DEM uncertainties has increased (Croke et al., 2013). The findings reported in Schaffrath et al. (2015) highlighted the importance of assessing DoD uncertainties as such, the calculated uncertainty was almost as high as the estimated net volume change. Consequently, numerous studies have implemented various methods for assessing the DoD uncertainty (e.g., Jones et al., 2013; Obu et al., 2017; Croke et al., 2013; Lallias-Tacon et al., 2014; Cavalli et al., 2017; Moretto et al., 2014; Schaffrath et al., 2015). Nevertheless, considering the number of DoD-based repeat ALS applications in the morphodynamics, the assessment of DoD uncertainty has been very limited. Furthermore, while a variety of approaches have been proposed and implemented, a consensus has yet to be built as to how DoD uncertainties should be quantified. While estimating and accounting for DoD uncertainties is important in morphodynamics, a detailed discussion is not within the scope of this paper. More detailed discussions can be found in a wide body of existing literature (e.g., Brasington et al., 2000, 2003; Carley et al., 2012; Fuller et al., 2003; Lane et al., 2003; Milan et al., 2007, 2011; Passalacqua et al., 2015; Vericat et al., 2017; Wheaton et al., 2010).

Multi-temporal ALS is most commonly used in landslide studies to produce DEMs that can be analyzed using straightforward differencing methods, DoD for example, to track ground motion and sediment displacement. This type of approach has already been shown to be more successful in locating and tracking landslides than other types of remote sensing approaches. However, as remote sensing data becomes increasingly available and more groups are familiarized with the use of ALS data, the applications for repeat ALS surveys of landslides are growing rapidly and being used to characterize more dynamic aspects of these events. Though many landslide studies focus on measuring the volume of sediment transported in these events and the progression of the event boundaries, some repeat ALS surveys have also been used to assess what parameters expedite or retard landslide progress. In particular, land cover and the availability of water can both affect landslide probabilities (Schmaltz et al., 2017; Tseng et al., 2013, 2015; Vehling et al., 2017). On the forefront of repeat ALS landslide research are the efforts to automate the detection and tracking of these hazards; however, research in this vein is nascent and has not yet been widely successful. Additionally, research into ways to more cleanly remove vegetation from landslide ALS data or to use vegetation to aid in the tracking of landslides is both a key challenge in the community and a necessary avenue for growth.

ALS change detection has undergone rapid adoption in the Earth sciences and has begun to assist in unlocking fundamental science questions related to dynamic Earth surface processes. Although significant progress has been made in applying ALS data to change detection, numerous approaches make fundamental assumptions that limit the full potential of this data for detecting 3D change and measuring deformation. For example, DoD is only 1D and neglects horizontal change, COSI-Corr is 2D- neglecting vertical change, and PIV can be 2.5D at best (e.g., Mukoyama, 2011). While ICP takes advantage of 3D data, it works on the basis of a rigid-body transformation. A rigid body transformation does not accurately model many natural phenomena, which limits its use in some fields (Krishnan et al., 2013). For instance, in neglecting inelastic strain caused by an earthquake or internal deformation of landslides and glacial flows, a rigid-body transformation cannot provide a complete picture of the real change in 3D. Consequently, neither of these approaches is able to fully capture most Earth science processes, which tend to be non-rigid and fully three-dimensional. There is however some emerging research on the use of non-rigid deformation approaches, such as coherent point drift (CPD) (Gadomski, 2016; Myronenko and Song, 2010), which uses a Gaussian Mixture Model to allow deformation to the point cloud between epochs. Alternative to measuring point cloud motion first, some research has attempted to start by constraining change detection using a physics based model of the process. Brooks et al. (2017) successfully used mobile laser scanning offsets constrained with an elastic deformation for the Napa Valley earthquake, but this coupling of models and 3D estimated deformation is still an emerging area of research. Wu et al. (2013) presented a multi-feature-based method that incorporates feature points, lines, and surface patches for robust co-registration of multiple surface models. Initial results of this non-rigid-transformation method showed its superiority over point-based methods and thus, deserves further attention as to its potential for ALS change detection studies. In addition, several other promising 3D point-based change detection methods, such as octree-based comparison algorithms (Barber et al., 2008; Girardeau-Montaut et al., 2005; Xu et al., 2015), 4-D filtering and calibration technique (Kromer et al., 2015), and integrated classification and change detection using machine learning (Tran et al., 2018) have been proposed. While the majority of these algorithms were developed for TLS, they can potentially be applied to repeat ALS data collections as well.

Apart from the rigid body nature of the transformation, ICP also has a few notable limitations in ALS change detection analysis. The performance of ICP largely depends on local topographic relief and the degree of alignment between pre- and post- event data when the transformation is initialized. In the absence of sufficient topographic structures, i.e., flat topography, a range of local transformations can provide acceptable alignment between point clouds and result in spurious change estimates (Scott et al., 2018). On the other hand, significant changes to the landscape (e.g., surface rupture or substantial erosion/deposition) also hamper the alignment between point clouds, rendering the use of ICP becomes virtually impossible. Therefore, an application-specific, optimal window size, which is a trade-off between a large scale to include sufficient topographic relief for accurate alignment and a small scale not to violate the rigid-body assumption, should be defined (Nissen et al., 2012). Krishnan et al. (2013) presented

a data-driven, iterative method to decide upon an appropriate window size for ICP. However, to date, the window size selection for ICP in ALS change detection studies has been rather arbitrary. To overcome some of the shortcoming associated with ICP, numerous, more complex adaptations of ICP have been proposed in the literature (Pomerleau et al., 2013). The method for treating outliers and penalizing the transformation for misalignments are generally the fundamental differences between ICP adaptations (Rusinkiewicz and Levoy, 2001). Therefore, different adaptations of the algorithm may not converge to a unique solution (change estimate) for the same paired lidar data (Pomerleau et al., 2013; Rusinkiewicz and Levoy, 2001), which poses a specific challenge as to which adaption should be preferred.

To date, most of the ALS change detection analysis has been performed using derived surface models, mainly DEMs along with intensity images to some extent, because such data are easier to process than 3D point clouds. These surface models require interpolation of irregularly spaced point data into regularly gridded data. However, the conversion results in a loss of information and precision regardless of the interpolation method. Resultantly, the final product resolution will be lower than the initial resolution of the point cloud. Furthermore, uncertainties in the surface representation are introduced during the conversion process (Passalacqua et al., 2015), which adversely affects the quality of change detection analysis. A number of factors such as point density and distribution, surface composition, topographic complexity, and interpolation method can contribute to surface representation uncertainty (Milan et al., 2011). However, the effect of surface representation uncertainty has not been extensively evaluated or discussed in ALS change detection studies. Nevertheless, with the awareness of these limitations, the Earth science community has demonstrated an increasing interest in using spatially-explicit point data, rather than gridded data products. So far, the most frequently implemented point-based analysis method in ALS change detection has been ICP. However, due to intrinsic limitations of the method, as discussed previously, ICP is not necessarily suitable for many Earth science sub-disciplines. For instance, the rigid-body assumption has been prohibitive in applying ICP for evaluating morphodynamics, particularly at finer scale. As such, ICP has not been successfully utilized in evaluating morphodynamics using repeat ALS so far, except for co-registration of data collections based on supposedly stable target areas. Similarly, ICP falls short of resolving 3D change in complex ecosystems and results in spurious change estimates along fault scarps or across landslides caused by seismic activity, where a simple vertical differencing has proven successful (e.g., Nissen et al., 2014). As an alternative to grid-based vertical differencing, Lague et al. (2013) introduced the Multi-scale Model-to-Model Cloud Comparison (M3C2) algorithm which allows direct differencing of point clouds and estimating vertical change without losing spatially explicit information. While the M3C2 algorithm was originally developed for TLS and successfully employed in several applications, the use of the algorithm in ALS change detection has been very limited and only one study has taken advantage of 3D point differencing in evaluating morphodynamics using repeat ALS data to date (Wagner et al., 2017).

The increasing interest in working directly with 3D point clouds, coupled with ever-increasing point density, brings new challenges regarding optimal storage and organization of repeat ALS data. The state-of-the-art concepts and techniques for managing massive point clouds have been reviewed highlighting both current challenges and future needs (Vo et al., 2016). Additionally, with increasing data volumes, data processing and subsequent change detection analysis using high density point clouds can become very computationally expensive. To this end a few studies have sought to offer new insights and presented promising results for efficient data processing and analysis to detect changes in massive point clouds (Richter et al., 2013b; Richter and Döllner, 2014). The continued improvements in laser scanning technology will likely lead to even larger data volumes and, thus, entail methodological challenges in addition to management challenges (Rieg et al., 2014; Vericat et al., 2017). The use of multi-temporal ALS data for change detection and monitoring purposes is, therefore, in need of novel and computationally efficient processing algorithms that transcend the ever-increasing volume and scale of laser scanning data (Vericat et al., 2017).

While new models and techniques will ultimately improve the results of 3D change detection, there are also still improvements to be made (a) providing the most accurate and consistent matches between irregular 3D point clouds, and (b) rigorously quantifying the level of uncertainty in the change detection estimates. Currently, change detection methodology does not consider anything beyond the 3D location of the points; information such as classification (ground, building, tree etc.) and return intensity are generally neglected. However, using hard target features, such as buildings, within the scene that can be identified and matched between epochs, analogous to the use of persistent scatterers in InSAR (e.g., Ferretti et al., 2004; Hooper et al., 2004), could improve registration between scans, resulting in more precise change detection estimates. Relatively few studies have taken this approach but Ekhtari and Glennie (2017), using buildings to register ALS data, and DeLong et al. (2015), using fence posts in TLS data, have both shown that it can be successful. A more thorough investigation of automatically detecting, modeling, and matching features in this way will more accurately constrain deformation in future studies.

Considering the number of repeat ALS change detection studies in the broad field of Earth sciences, quantification of uncertainty in change detection results has been very limited and typically restricted to DoD analysis. One exception to this is Scott et al. (2018), which introduces an empirical error metric, to evaluate the relative quality of ICP displacement estimates. While individual DEM and propagated DoD uncertainties have commonly been expressed as a single value for the entire grid, these uncertainties are unlikely to be spatially uniform. Estimating spatially variable DEM uncertainty, however, is not a trivial task, particularly in the absence of high quality auxiliary data. Although Wheaton et al. (2010) proposed a fuzzy inference system (FIS) in an effort to fill this gap, this method has yet to be widely implemented in ALS-change detection studies. Additionally, with increasing interest in using 3D data, rather than derived gridded data products, assessment of spatially variable uncertainty in point clouds has gained some traction. Some initial work in this area has been presented in Hartzell et al. (2015), for modeling snow volume uncertainty, and in Zhang et al. (2015), for estimating earthquake deformation. However, the approaches used in both studies required detailed modeling of the laser scanning equipment, scanning geometry, and raw observations which would not be possible for many Earth science applications. This type of rigorous error propagation will rely on ALS vendors providing estimates of per point accuracy that can then be applied to the resultant change detection estimates. Additionally, beyond point accuracy measures, a study of the effect that filtering and gridding of the raw point cloud observations have on the overall change detection accuracy would also improve the quantification of uncertainty for a wide breadth of research.

Although the cost of data acquisition is declining as ALS becomes more pervasive, it is still expensive. Furthermore, the existence of pre- and post-event ALS data is still uncommon for many isolated hazard events, such as earthquakes, volcanic eruptions, wildfires, landslides, etc. Consequently, data availability is still a major limitation for many ALS change detection applications, particularly for large areal coverage and continuous monitoring purposes. Nevertheless, projects like the “B4”, which collected ALS data for the San Andreas fault (Bevis et al., 2005) or similar projects in Japan acquired ALS data across the potential epicentral regions of future earthquakes (Nissen et al., 2014) demonstrate that repeat ALS data are increasingly being used as a standard investigative tool. To date, the ALS data within the scope of Earth sciences have traditionally been collected from either fixed-wing aircrafts or helicopters, which adversely affect the cost and frequency of

data collection. Compared to traditional ALS, UAVs could potentially provide more flexibility in terms of flight frequency and design, and lower acquisition cost at small spatial extents. However, until recently the UAV-based lidar has lagged behind due mainly to low positional accuracy, point density, and the limited range of light-weight systems. Recent and rapid developments in sensor technology are beginning to allow the implementation of miniaturized lidar systems capable of acquiring quality data from UAVs. A recent pilot study has evaluated a survey-grade, long-range UAV-based lidar system and provided valuable insight as to data calibration, processing, and analysis (Starek et al., 2018). The experimental results presented in this study are promising and demonstrate the improvements in the new technology. While it is currently in its infancy, the use of UAV-based lidar has a great potential to open doors for new applications in airborne change detection. For instance, UAV-based lidar would considerably lower the risk of data collection in volcanic areas or around other hazard types and would provide rapid response capabilities for many isolated events. Nevertheless, considering the flight endurance, spatial coverage, and superior sensor characteristics, traditional ALS data collected from fixed-winged aircraft and helicopters will still be at the forefront of change detection studies in near future.

5. Conclusions

Despite the increasing number of studies, ALS change detection represents a small subset of lidar applications in the Earth sciences. Currently, multi-temporal ALS data are primarily used in studies concerning geomorphology and morphodynamics, landslide and earthquake surface displacement, and above-ground biomass dynamics. They have also been used selectively in volcanology and cryosphere science. Although significant progress has been made in applying ALS data to change detection, numerous approaches make fundamental assumptions that limit the use of this data for detecting fully 3D change and thus, the full potential of repeat ALS in Earth sciences has yet to be realized. The use of multi-temporal ALS data for change detection and monitoring purposes is, therefore, in need of novel and computationally efficient processing algorithms. In addition, the continued improvements in lidar technology will likely lead to larger data volumes and, thus, entail data management challenges. Currently, change detection methodology does not consider anything beyond the 3D location of the points; information such as classification and return intensity are generally neglected. Incorporating such information into change detection analyses will potentially improve the applicability, quantitative accuracy, and informative value of ALS change detection. Quantification of uncertainty in change detection results is also an area that requires further attention, as it is vitally important to understanding what 3D differences detected between epochs represent actual change as opposed to noise. The existence of pre- and post-event ALS data is still uncommon for many isolated hazard events, such as earthquakes, volcanic eruptions, wildfires, landslides, etc. Consequently, data availability is still a major limitation for many ALS change detection applications. To date, a majority of the estimates of ALS change detection result from the analysis of only two epochs of observations – often a pre- and post-event dataset. With the increasing availability of low cost lidar data, as well as 3D data derived from stereo photography, it would appear that future studies could benefit from taking advantage of multiple temporally spaced 3D datasets to both improve prediction and drive down estimated error in a similar manner to that employed with stacked radar interferograms. ALS has become increasingly integral to change detection across the Earth sciences and this trend will continue as repeat ALS data coverage becomes more widespread and accessible.

Acknowledgments

Partial support for all authors was provided through a grant from the National Science Foundation Earth Sciences: Instrumentation and Facilities (EAR/IF) program (Grant #1339015 and #1338994).

References

Abermann, J., Fischer, A., Lambrecht, A., Geist, T., 2010. On the potential of very high-resolution repeat DEMs in glacial and periglacial environments. Cryosph 4, 53–65. https://doi.org/10.5194/tc-4-53-2010.

Alonzo, M., Morton, D.C., Cook, B.D., Andersen, H.-E., Babcock, C., Pattison, R., 2017. Patterns of canopy and surface layer consumption in a boreal forest fire from repeat airborne LiDAR. Environ. Res. Lett. 12, 065004. https://doi.org/10.1088/1748-9326/aa6ade.

Andersen, H.-E., Reutebuch, S.E., McGaughey, R.J., D'Oliveira, M.V.N., Keller, M., 2014. Monitoring selective logging in western Amazonia with repeat LiDAR flights. Remote Sens. Environ. 151, 157–165. https://doi.org/10.1016/j.rse.2013.08.049.

Anderson, S., Pitlick, J., 2014. Using repeat LiDAR to estimate sediment transport in a steep stream. J. Geophys. Res. Earth Surf. 119, 621–643. https://doi.org/10.1002/2013JF002933.

Anderson, S.W., Anderson, S.P., Anderson, R.S., 2015. Exhumation by debris flows in the 2013 Colorado front range storm. Geology 43, 391–394. https://doi.org/10.1130/G36507.1.

Barber, D., Holland, D., Mills, J., 2008. Change detection for topographic mapping using three- dimensional data structures. Int. Arch. Photogramm. Remote. Sens. Spat. Inf. Sci. XXXVII, 1177–1182.

Behncke, B., Fornaciai, A., Neri, M., Favalli, M., Ganci, G., Mazzarini, F., 2016. LiDAR surveys reveal eruptive volumes and rates at Etna, 2007–2010. Geophys. Res. Lett. 43, 4270–4278. https://doi.org/10.1002/2016GL068495.

Besl, P.J., McKay, N.D., 1992. A method for registration of 3-D Shapes. IEEE Trans. Pattern Anal. Mach. Intell. https://doi.org/10.1117/12.57955.

Bevis, M., Hudnut, K., Sanchez, R., Toth, C., Grejner-Brzezinska, D., Kendrick, E., Caccamise, D., Raleigh, D., Zhou, H., Shan, S., Shindle, W., Yong, A., Harvey, J., Borsa, A., Ayoub, F., Shrestha, R., Carter, B., Sartori, M., Phillips, D., Coloma, F., 2005. The B4 project: scanning the San Andreas and San Jacinto fault zones. EOS Trans. Am. Geophys. Union 86, H34B–01.

Boehm, H.-D.V., Liesenberg, V., Limin, S.H., 2013. Multi-temporal airborne LiDAR-survey and field measurements of tropical peat swamp forest to monitor changes. IEEE J. Sel. Top. Appl. Earth Obs. Remote Sens. 6, 1524–1530. https://doi.org/10.1109/JSTARS.2013.2258895.

Bohlin, I., Olsson, H., Bohlin, J., Granström, A., 2017. Quantifying post-fire fallen trees using multi-temporal lidar. Int. J. Appl. Earth Obs. Geoinf. 63, 186–195. https://doi.org/10.1016/j.jag.2017.08.004.

Bollandsås, O.M., Gregoire, T.G., Næsset, E., Øyen, B.H., 2013. Detection of biomass change in a Norwegian mountain forest area using small footprint airborne laser scanner data. Stat. Methods Appl. 22, 113–129. https://doi.org/10.1007/s10260-012-0220-5.

Bollmann, E., 2010. Airborne Laser Scanning Glacier Mass Balance (Master's Thesis). University of Innsbruck.

Borsa, A., Minster, J.B., 2012. Rapid determination of near-fault earthquake deformation using differential LiDAR. Bull. Seismol. Soc. Am. 102, 1335–1347. https://doi.org/10.1785/0120110159.

Brasington, J., Rumsby, B.T., McVey, R.A., 2000. Monitoring and modelling morphological change in a braided gravel-bed river using high resolution GPS-based survey. Earth Surf. Process. Landf. 25, 973–990. https://doi.org/10.1002/1096-9837(200008)25:9<973::AID-ESP111>3.0.CO;2-Y.

Brasington, J., Langham, J., Rumsby, B., 2003. Methodological sensitivity of morphometric estimates of coarse fluvial sediment transport. Geomorphology 53, 299–316. https://doi.org/10.1016/S0169-555X(02)00320-3.

Brock, J.C., Krabill, W.B., Sallenger, A.H., 2004. Barrier island morphodynamic classification based on LiDAR metrics for North Assateague Island, Maryland. J. Coast. Res. 20, 498–509. https://doi.org/10.2112/1551-5036(2004)020[0498:BIMCBO]2.0.CO;2.

Brooks, B.A., Minson, S.E., Glennie, C.L., Nevitt, J.M., Dawson, T., Rubin, R., Ericksen, T.L., Lockner, D., Hudnut, K., Langenheim, V., Lutz, A., Mareschal, M., Murray, J., Schwartz, D., Zaccone, D., 2017. Buried shallow fault slip from the South Napa earthquake revealed by near-field geodesy. Sci. Adv. 3, 1–12. https://doi.org/10.1126/sciadv.1700525.

Bull, J.M., Miller, H., Gravley, D.M., Costello, D., Hikuroa, D.C.H., Dix, J.K., 2010. Assessing debris flows using LiDAR differencing: 18 May 2005 Matata event, New Zealand. Geomorphology 124, 75–84. https://doi.org/10.1016/j.geomorph.2010.08.011.

Burns, W.J., Coe, J.A., Kaya, B.S., Ma, L., 2010. Analysis of elevation changes detected from multi-temporal LiDAR surveys in forested landslide terrain in western Oregon. Environ. Eng. Geosci. 16, 315–341. https://doi.org/10.2113/gseegeosci.16.4.315.

Burvingt, O., Masselink, G., Russell, P., Scott, T., 2017. Classification of beach response to extreme storms. Geomorphology 295, 722–737. https://doi.org/10.1016/j.geomorph.2017.07.022.

Campbell, L.B., Coops, N.C., Saunders, S.C., 2017. LiDAR as an advanced remote sensing technology to augment ecosystem classification and mapping. J. Ecosyst. Manag. 17, 1–13.

Cao, L., Coops, N.C., Innes, J.L., Sheppard, S.R.J., Fu, L., Ruan, H., She, G., 2016. Estimation of forest biomass dynamics in subtropical forests using multi-temporal airborne LiDAR data. Remote Sens. Environ. 178, 158–171. https://doi.org/10.1016/j.rse.2016.03.012.

Carley, J.K., Pasternack, G.B., Wyrick, J.R., Barker, J.R., Bratovich, P.M., Massa, D.A., Reedy, G.D., Johnson, T.R., 2012. Significant decadal channel change 58-67 years post-dam accounting for uncertainty in topographic change detection between

contour maps and point cloud models. Geomorphology 179, 71–88. https://doi.org/10.1016/j.geomorph.2012.08.001.
Cavalli, M., Goldin, B., Comiti, F., Brardinoni, F., Marchi, L., 2017. Assessment of erosion and deposition in steep mountain basins by differencing sequential digital terrain models. Geomorphology 291, 4–16. https://doi.org/10.1016/j.geomorph.2016.04.009.
Charlton, M.E., Large, A.R.G., Fuller, I.C., 2003. Application of airborne LiDAR in river environments: the River Coquet, Northumberland, UK. Earth Surf. Process. Landf. 28, 299–306. https://doi.org/10.1002/esp.482.
Chen, G., Ozelkan, E., Singh, K.K., Zhou, J., Brown, M.R., Meentemeyer, R.K., 2017. Uncertainties in mapping forest carbon in urban ecosystems. J. Environ. Manag. 187, 229–238. https://doi.org/10.1016/j.jenvman.2016.11.062.
Clark, K.J., Nissen, E.K., Howarth, J.D., Hamling, I.J., Mountjoy, J.J., Ries, W.F., Jones, K., Goldstien, S., Cochran, U.A., Villamor, P., Hreinsdóttir, S., Litchfield, N.J., Mueller, C., Berryman, K.R., Strong, D.T., 2017. Highly variable coastal deformation in the 2016 MW7.8 Kaikōura earthquake reflects rupture complexity along a transpressional plate boundary. Earth Planet. Sci. Lett. 474, 334–344. https://doi.org/10.1016/j.epsl.2017.06.048.
Coppin, P., Jonckheere, I., Nackaerts, K., Muys, B., Lambin, E., 2004. Digital change detection methods in ecosystem monitoring: a review. Int. J. Remote Sens. 25, 1565–1596. https://doi.org/10.1080/0143116031000101675.
Corsini, A., Borgatti, L., Cervi, F., Dahne, A., Ronchetti, F., Sterzai, P., 2009. Estimating mass-wasting processes in active earth slides – earth flows with time-series of high-resolution DEMs from photogrammetry and airborne LiDAR. Nat. Hazards Earth Syst. Sci. 9, 433–439. https://doi.org/10.5194/nhess-9-433-2009.
Croke, J., Todd, P., Thompson, C., Watson, F., Denham, R., Khanal, G., 2013. The use of multi-temporal LiDAR to assess basin-scale erosion and deposition following the catastrophic January 2011 Lockyer flood, SE Queensland, Australia. Geomorphology 184, 111–126. https://doi.org/10.1016/j.geomorph.2012.11.023.
Crookston, N.L., Finley, A.O., 2008. yaImpute: an R Package for k NN Imputation. J. Stat. Softw. 23.
Daehne, A., Corsini, A., 2013. Kinematics of active earthflows revealed by digital image correlation and DEM subtraction techniques applied to multi-temporal LiDAR data. Earth Surf. Process. Landf. 38, 640–654. https://doi.org/10.1002/esp.3351.
DeBeer, C.M., Pomeroy, J.W., 2010. Simulation of the snowmelt runoff contributing area in a small alpine basin. Hydrol. Earth Syst. Sci. 14, 1205–1219. https://doi.org/10.5194/hess-14-1205-2010.
Deems, J.S., Painter, T.H., Finnegan, D.C., 2013. LiDAR measurement of snow depth: a review. J. Glaciol. 59, 467–479. https://doi.org/10.3189/2013JoG12J154.
DeLong, S.B., Prentice, C.S., Hilley, G.E., Ebert, Y., 2012. Multi-temporal ALSM change detection, sediment delivery, and process mapping at an active earthflow. Earth Surf. Process. Landf. 37, 262–272. https://doi.org/10.1002/esp.2234.
DeLong, S.B., Lienkaemper, J.J., Pickering, A.J., Avdievitch, N.N., 2015. Rates and patterns of surface deformation from laser scanning following the South Napa earthquake, California. Geosphere 11, 2015–2030. https://doi.org/10.1130/GES01189.1.
Dong, P., 2015. Automated measurement of sand dune migration using multi-temporal LiDAR data and GIS. Int. J. Remote Sens. 36, 5426–5447. https://doi.org/10.1080/01431161.2015.1093192.
Dubayah, R.O., Sheldon, S.L., Clark, D.B., Hofton, M.A., Blair, J.B., Hurtt, G.C., Chazdon, R.L., 2010. Estimation of tropical forest height and biomass dynamics using lidar remote sensing at la Selva, Costa Rica. J. Geophys. Res. Biogeosci. 115, 1–17. https://doi.org/10.1029/2009JG000933.
Duffy, B., Quigley, M., Barrell, D.J.A., Van Dissen, R., Stahl, T., Leprince, S., McInnes, C., Bilderback, E., 2013. Fault kinematics and surface deformation across a releasing bend during the 2010 MW 7.1 Darfield, New Zealand, earthquake revealed by differential LiDAR and cadastral surveying. Bull. Geol. Soc. Am. 125, 420–431. https://doi.org/10.1130/B30753.1.
Eitel, J.U.H., Höfle, B., Vierling, L.A., Abellán, A., Asner, G.P., Deems, J.S., Glennie, C.L., Joerg, P.C., LeWinter, A.L., Magney, T.S., Mandlburger, G., Morton, D.C., Müller, J., Vierling, K.T., 2016. Beyond 3-D: the new spectrum of LiDAR applications for earth and ecological sciences. Remote Sens. Environ. 186, 372–392. https://doi.org/10.1016/j.rse.2016.08.018.
Ekhtari, N., Glennie, C.L., 2017. High-resolution mapping of near-field deformation with airborne Earth observation data, a comparison study. IEEE Trans. Geosci. Remote Sens. https://doi.org/10.1109/TGRS.2017.2765601.
Engelkemeir, R.M., Khan, S.D., 2008. Lidar mapping of faults in Houston, Texas, USA. Geosphere 4, 170–182. https://doi.org/10.1130/GES00096.1.
Englhart, S., Jubanski, J., Siegert, F., 2013. Quantifying dynamics in tropical peat swamp forest biomass with multi-temporal LiDAR datasets. Remote Sens. 5, 2368–2388. https://doi.org/10.3390/rs5052368.
Favalli, M., Fornaciai, A., Pareschi, M.T., 2009. LIDAR strip adjustment: application to volcanic areas. Geomorphology 111, 123–135. https://doi.org/10.1016/j.geomorph.2009.04.010.
Favalli, M., Fornaciai, A., Mazzarini, F., Harris, A.J.L., Neri, M., Behncke, B., Pareschi, M.T., Tarquini, S., Boschi, E., 2010a. Evolution of an active lava flow field using a multi-temporal LiDAR acquisition. J. Geophys. Res. Solid Earth 115, 1–17. https://doi.org/10.1029/2010JB007463.
Favalli, M., Harris, A.J.L., Fornaciai, A., Pareschi, M.T., Mazzarini, F., 2010b. The distal segment of Etna's 2001 basaltic lava flow. Bull. Volcanol. 72, 119–127. https://doi.org/10.1007/s00445-009-0300-z.
Fernandez Diaz, J.C., Okyay, U., Glennie, C.L., 2018. Surface Deformation at Yellowstone Caldera: Observations from Repeat ALS between 2008 and 2017, Abstract G51C-0506 Presented at Fall Meeting. AGU.
Fernandez-Diaz, J.C., Carter, W.E., Glennie, C., Shrestha, R.L., Pan, Z., Ekhtari, N., Singhania, A., Hauser, D., Sartori, M., 2016. Capability assessment and performance metrics for the titan multispectral mapping lidar. Remote Sens. 8, 1–33. https://doi.org/10.3390/rs8110936.
Ferretti, a., Novali, F., Bürgmann, R., Hilley, G., Prati, C., 2004. InSAR permanent scatterer analysis reveals ups and downs in San Francisco Bay Area. EOS Trans. Am. Geophys. Union 85, 317. https://doi.org/10.1029/2004EO340002.
Fornaciai, A., Behncke, B., Favalli, M., Neri, M., Tarquini, S., Boschi, E., 2010. Detecting short-term evolution of Etnean scoria cones: a LiDAR-based approach. Bull. Volcanol. 72, 1209–1222. https://doi.org/10.1007/s00445-010-0394-3.
Fritzmann, P., Höfle, B., Vetter, M., Sailer, R., Stötter, J., Bollmann, E., 2011. Surface classification based on multi-temporal airborne LiDAR intensity data in high mountain environments: a case study from Hintereisferner, Austria. Z. Geomorphol. 55, 105–126. https://doi.org/10.1127/0372-8854/2011/0055S2-0048.
Fuller, I.C., Large, A.R.G., Charlton, M.E., Heritage, G.L., Milan, D.J., 2003. Reach-scale sediment transfers: an evaluation of two morphological budgeting approaches. Earth Surf. Process. Landf. 28, 889–903. https://doi.org/10.1002/esp.1011.
Gadomski, P.J., 2016. Measuring Glacier Surface Velocities with Lidar: A Comparison of Three-Dimensional Change Detection Methods (Master's Thesis). University of Houston.
Geist, T., Lutz, E., Stoetter, J., 2003. Airborne laser scanning technology and its potential for applications in glaciology. In: ISPRS Work. 3-D Reconstr. From Airborne Laserscanner Insa. Data 0–5.
Ghuffar, S., Székely, B., Roncat, A., Pfeifer, N., 2013. Landslide displacement monitoring using 3D range flow on airborne and terrestrial LiDAR data. Remote Sens. 5, 2720–2745. https://doi.org/10.3390/rs5062720.
Girardeau-Montaut, D., Roux, M., Marc, R., Thibault, G., 2005. Change detection on points cloud data acquired with a ground laser scanner. In: Proc. ISPRS Work. Laser Scanning WG III/3–4, pp. 30–35.
Glennie, C.L., 2007. Rigorous 3D error analysis of kinematic scanning LIDAR systems. J. Appl. Geod. 1, 147–157. https://doi.org/10.1515/jag.2007.017.
Glennie, C.L., Hinojosa-Corona, A., Nissen, E., Kusari, A., Oskin, M.E., Arrowsmith, J.R., Borsa, A., 2014. Optimization of legacy LiDAR data sets for measuring near-field earthquake displacements. Geophys. Res. Lett. 41, 3494–3501. https://doi.org/10.1002/2014GL059919.
Greaves, H.E., Vierling, L.A., Eitel, J.U.H., Boelman, N.T., Magney, T.S., Prager, C.M., Griffin, K.L., 2017. Applying terrestrial lidar for evaluation and calibration of airborne lidar-derived shrub biomass estimates in Arctic tundra. Remote Sens. Lett. 8, 175–184. https://doi.org/10.1080/2150704X.2016.1246770.
Hansen, M.C., Loveland, T.R., 2012. A review of large area monitoring of land cover change using Landsat data. Remote Sens. Environ. 122, 66–74. https://doi.org/10.1016/j.rse.2011.08.024.
Harpold, A.A., Marshall, J.A., Lyon, S.W., Barnhart, T.B., Fisher, B.A., Donovan, M., Brubaker, K.M., Crosby, C.J., Glenn, N.F., Glennie, C.L., Kirchner, P.B., Lam, N., Mankoff, K.D., McCreight, J.L., Molotch, N.P., Musselman, K.N., Pelletier, J., Russo, T., Sangireddy, H., Sjöberg, Y., Swetnam, T., West, N., 2015. Laser vision: lidar as a transformative tool to advance critical zone science. Hydrol. Earth Syst. Sci. 19, 2881–2897. https://doi.org/10.5194/hess-19-2881-2015.
Harris, A.J.L., Favalli, M., Steffke, A., Fornaciai, A., Boschi, E., 2010. A relation between lava discharge rate, thermal insulation, and flow area set using LiDAR data. Geophys. Res. Lett. 37, 1–7. https://doi.org/10.1029/2010GL044683.
Hartzell, P.J., Gadomski, P.J., Glennie, C.L., Finnegan, D.C., Deems, J.S., 2015. Rigorous error propagation for terrestrial laser scanning with application to snow volume uncertainty. J. Glaciol. 61, 1147–1158. https://doi.org/10.3189/2015JoG15J031.
Hodgetts, D., 2013. Laser scanning and digital outcrop geology in the petroleum industry: a review. Mar. Pet. Geol. 46, 335–354. https://doi.org/10.1016/j.marpetgeo.2013.02.014.
Höfle, B., Rutzinger, M., 2011. Topographic airborne LiDAR in geomorphology: a technological perspective. Z. Geomorphol. 55, 1–29. https://doi.org/10.1127/0372-8854/2011/0055S2-0043.
Hooper, A., Zebker, H., Segall, P., Kampes, B., 2004. A new method for measuring deformation on volcanoes and other natural terrains using InSAR persistent scatterers. Geophys. Res. Lett. 31, 1–5. https://doi.org/10.1029/2004GL021737.
Hopkinson, C., Demuth, M.N., 2006. Using airborne LiDAR to assess the influence of glacier downwasting on water resources in the Canadian Rocky Mountains. Can. J. Remote Sens. 32, 212–222. https://doi.org/10.5589/m06-012.
Hudak, A.T., Strand, E.K., Vierling, L.A., Byrne, J.C., Eitel, J.U.H., Martinuzzi, S., Falkowski, M.J., 2012. Quantifying aboveground forest carbon pools and fluxes from repeat LiDAR surveys. Remote Sens. Environ. 123, 25–40. https://doi.org/10.1016/j.rse.2012.02.023.
Hudnut, K.W., Borsa, A., Glennie, C.L., Minster, J.B., 2002. High-resolution topography along surface rupture of the 16 October 1999 Hector Mine, California, Earthquake (Mw 7.1) from Airborne Laser Swath Mapping. Bull. Seismol. Soc. Am. 92, 1570–1576. https://doi.org/10.1785/0120000934.
Irvine-Fynn, T.D.L., Barrand, N.E., Porter, P.R., Hodson, A.J., Murray, T., 2011. Recent high-arctic glacial sediment redistribution: a process perspective using airborne LiDAR. Geomorphology 125, 27–39. https://doi.org/10.1016/j.geomorph.2010.08.012.
Jaboyedoff, M., Oppikofer, T., Abellán, A., Derron, M.H., Loye, A., Metzger, R., Pedrazzini, A., 2012. Use of LiDAR in landslide investigations: a review. Nat. Hazards 61, 5–28. https://doi.org/10.1007/s11069-010-9634-2.
Jensen, J.L.R., Humes, K.S., Vierling, L.A., Hudak, A.T., 2008. Discrete return lidar-based prediction of leaf area index in two conifer forests. Remote Sens. Environ. 112, 3947–3957. https://doi.org/10.1016/j.rse.2008.07.001.
Jianya, G., Haigang, S., Guorui, M., Qiming, Z., 2008. A review of multi-temporal remote sensing data change detection algorithms. In: The International Archives of the Photogrammetry, Remote Sensing, and Spatial Information Sciences Sciences, pp. 757–762 (Beijing, China).
Joerg, P.C., Morsdorf, F., Zemp, M., 2012. Uncertainty assessment of multi-temporal

airborne laser scanning data: a case study on an Alpine glacier. Remote Sens. Environ. 127, 118–129. https://doi.org/10.1016/j.rse.2012.08.012.
Jones, B.M., Stoker, J.M., Gibbs, A.E., Grosse, G., Romanovsky, V.E., Douglas, T.A., Kinsman, N.E.M., Richmond, B.M., 2013. Quantifying landscape change in an arctic coastal lowland using repeat airborne LiDAR. Environ. Res. Lett. 8, 1–10. https://doi.org/10.1088/1748-9326/8/4/045025.
Joyce, K.E., Samsonov, S., Manville, V., Jongens, R., Graettinger, A., Cronin, S.J., 2009. Remote sensing data types and techniques for lahar path detection: a case study at Mt Ruapehu, New Zealand. Remote Sens. Environ. 113, 1778–1786. https://doi.org/10.1016/j.rse.2009.04.001.
Keane, R.D., Adrian, R.J., 1992. Theory of cross-correlation analysis of PIV images. Appl. Sci. Res. 49, 191–215.
Keeley, J.E., 2009. Fire intensity, fire severity and burn severity: a brief review and suggested usage. Int. J. Wildland Fire 18, 116. https://doi.org/10.1071/wf07049.
Kennett, M., Eiken, T., 1997. Airborne measurement of glacier surface elevation by scanning laser altimeter. Ann. Glaciol. 24, 293–296.
Knoll, C., Kerschner, H., 2009. A glacier inventory for South Tyrol, Italy, based on airborne laser-scanner data. Ann. Glaciol. 50, 46–52. https://doi.org/10.3189/172756410790595903.
Kodde, M., Pfeifer, N., Gorte, B.G.H., Geist, T., Holfe, B., Höfle, B., 2007. Automatic glacier surface analysis from airborne laser scanning. In: The International Archives of Photogrammetry, Remote Sensing, and Spatial Information Sciences, pp. 221–226 (Espoo, Finland).
Krishnan, A.K., Nissen, E., Saripalli, S., Arrowsmith, J.R., Hinojosa-Corona, A., 2013. Change detection using airborne LiDAR: applications to earthquakes. In: Experimental Robotics: The 13th International Symposium on Experimental Robotics (Springer Tracts in Advanced Robotics), pp. 733–743. https://doi.org/10.1007/978-3-319-00065-7_49.
Kromer, R.A., Abellán, A., Hutchinson, D.J., Lato, M., Edwards, T., Jaboyedoff, M., 2015. A 4D filtering and calibration technique for small-scale point cloud change detection with a terrestrial laser scanner. Remote Sens. 7, 13029–13058. https://doi.org/10.3390/rs71013029.
Kusari, A., Glennie, C.L., Brooks, B.A., Ericksen, T.L., 2019. Precise registration of laser mapping data by planar feature extraction for deformation monitoring. IEEE Trans. Geosci. Remote Sens. 57, 3404–3422. https://doi.org/10.1109/TGRS.2018.2884712.
Lague, D., Brodu, N., Leroux, J., 2013. Accurate 3D comparison of complex topography with terrestrial laser scanner: application to the Rangitikei canyon (N-Z). ISPRS J. Photogramm. Remote Sens. 82, 10–26. https://doi.org/10.1016/j.isprsjprs.2013.04.009.
Lallias-Tacon, S., Liébault, F., Piégay, H., 2014. Step by step error assessment in braided river sediment budget using airborne LiDAR data. Geomorphology 214, 307–323. https://doi.org/10.1016/j.geomorph.2014.02.014.
Lane, S.N., Westaway, R.M., Hicks, D.M., 2003. Estimation of erosion and deposition volumes in a large, gravel-bed, braided river using synoptic remote sensing. Earth Surf. Process. Landf. 28, 249–271. https://doi.org/10.1002/esp.483.
Legleiter, C.J., 2012. Remote measurement of river morphology via fusion of LiDAR topography and spectrally based bathymetry. Earth Surf. Process. Landf. 37, 499–518. https://doi.org/10.1002/esp.2262.
Leprince, S., Ayoub, F., Klinger, Y., Avouac, J.-P., 2007. Co-Registration of Optically Sensed Images and Correlation (COSI-Corr): An operational methodology for ground deformation measurements. In: 2007 IEEE International Geoscience and Remote Sensing Symposium. IEEE, pp. 1943–1946. https://doi.org/10.1109/IGARSS.2007.4423207.
Leprince, S., Hudnut, K.W., Akciz, S., Hinojosa-Corona, A., Fletcher, J.M., 2011. Surface Rupture and Slip Variation Induced by the 2010 El Mayor – Cucapah Earthquake, Baja California, Quantified Using COSI-Corr Analysis on Pre- and Post-Earthquake LiDAR Acquisitions, Abstract EP41A-0596 presented at 2011 Fall Meeting. AGU.
Levoy, F., Anthony, E.J., Monfort, O., Robin, N., Bretel, P., 2013. Formation and migration of transverse bars along a tidal sandy coast deduced from multi-temporal LiDAR datasets. Mar. Geol. 342, 39–52. https://doi.org/10.1016/j.margeo.2013.06.007.
Li, A., Glenn, N.F., Olsoy, P.J., Mitchell, J.J., Shrestha, R., 2015. Aboveground biomass estimates of sagebrush using terrestrial and airborne LiDAR data in a dryland ecosystem. Agric. For. Meteorol. 213, 138–147. https://doi.org/10.1016/j.agrformet.2015.06.005.
Liu, H., Wang, L., Sherman, D.J., Gao, Y., Wu, Q., 2010. An object-based conceptual framework and computational method for representing and analyzing coastal morphological changes. Int. J. Geogr. Inf. Sci. 24, 1015–1041. https://doi.org/10.1080/13658810903270569.
Lu, D., Mausel, P., Brondízio, E., Moran, E., 2004. Change detection techniques. Int. J. Remote Sens. 25, 2365–2401. https://doi.org/10.1080/0143116031000139863.
Lyda, A.W., Zhang, X., Glennie, C.L., Hudnut, K.W., Brooks, B.A., 2016. Airborne light detection and ranging (LiDAR) derived deformation from the Mw 6.0 24 August, 2014 South Napa earthquake estimated by two and three dimensional point cloud change detection techniques. In: The International Archives of the Photogrammetry, Remote Sensing and Spatial Information Sciences, pp. 35–42. https://doi.org/10.5194/isprsarchives-XLI-B2-35-2016. (Prague, Czech Republic).
Marenco, F., Johnson, B., Turnbull, K., Newman, S., Haywood, J., Webster, H., Ricketts, H., 2011. Airborne lidar observations of the 2010 Eyjafjallajkull volcanic ash plume. J. Geophys. Res. Atmos. 116, 1–15. https://doi.org/10.1029/2011JD016396.
McCarley, T.R., Kolden, C.A., Vaillant, N.M., Hudak, A.T., Smith, A.M.S., Kreitler, J., 2017a. Landscape-scale quantification of fire-induced change in canopy cover following mountain pine beetle outbreak and timber harvest. For. Ecol. Manag. 391, 164–175. https://doi.org/10.1016/j.foreco.2017.02.015.
McCarley, T.R., Kolden, C.A., Vaillant, N.M., Hudak, A.T., Smith, A.M.S., Wing, B.M., Kellogg, B.S., Kreitler, J., 2017b. Multi-temporal LiDAR and Landsat quantification of fire-induced changes to forest structure. Remote Sens. Environ. 191, 419–432. https://doi.org/10.1016/j.rse.2016.12.022.
McRoberts, R.E., Bollandsås, O.M., Næsset, E., 2014. Modeling and estimating change. In: Maltamo, M., Næsset, E., Vauhkonen, J. (Eds.), Forestry Applications of Airborne Laser Scanning: Concepts and Case Studies. Springer, Netherlands, Dordrecht, pp. 293–313. https://doi.org/10.1007/978-94-017-8663-8_15.
McRoberts, R.E., Næsset, E., Gobakken, T., Bollandsås, O.M., 2015. Indirect and direct estimation of forest biomass change using forest inventory and airborne laser scanning data. Remote Sens. Environ. 164, 36–42. https://doi.org/10.1016/j.rse.2015.02.018.
Meigs, A., 2013. Active tectonics and the LiDAR revolution. Lithosphere 5, 226–229. https://doi.org/10.1130/RF.L004.1.
Meredith, A., Eslinger, D., Aurin, D., 1999. An Evaluation of Hurricane-Induced Erosion along the North Carolina Coast Using Airborne LiDAR Surveys, NOAA Coastal Services Center Technical Report/99031-PUB.
Meyer, V., Saatchi, S.S., Chave, J., Dalling, J.W., Bohlman, S., Fricker, G.A., Robinson, C., Neumann, M., Hubbell, S.P., 2013. Detecting tropical forest biomass dynamics from repeated airborne lidar measurements. Biogeosciences 10, 5421–5438. https://doi.org/10.5194/bg-10-5421-2013.
Milan, D.J., Heritage, G.L., Hetherington, D., 2007. Application of a 3D laser scanner in the assessment of erosion and deposition volumes and channel change in a proglacial river. Earth Surf. Process. Landf. 32, 1657–1674. https://doi.org/10.1002/esp.1592.
Milan, D.J., Heritage, G.L., Large, A.R.G., Fuller, I.C., 2011. Filtering spatial error from DEMs: implications for morphological change estimation. Geomorphology 125, 160–171. https://doi.org/10.1016/j.geomorph.2010.09.012.
Milliner, C.W.D., Dolan, J.F., Hollingsworth, J., Leprince, S., Ayoub, F., Sammis, C.G., 2015. Quantifying near-field and off-fault deformation patterns of the 1992 M w 7.3 Landers earthquake. Geochem. Geophys. Geosyst. 16, 1577–1598. https://doi.org/10.1002/2014GC005693.
Milliner, C.W.D., Dolan, J.F., Hollingsworth, J., Leprince, S., Ayoub, F., 2016. Comparison of coseismic near-field and off-fault surface deformation patterns of the 1992 M w 7.3 Landers and 1999 M w 7.1 Hector Mine earthquakes: implications for controls on the distribution of surface strain. Geophys. Res. Lett. 43, 10,115–10,124. https://doi.org/10.1002/2016GL069841.
Mitasova, H., Drake, T.G., Bernstein, D.J., Harmon, R.S., 2004. Quantifying rapid changes in coastal topography using modern mapping techniques and Geographic Information System. Environ. Eng. Geosci. 10, 1–11.
Mitasova, H., Overton, M.F., Recalde, J.J., Bernstein, D.J., Freeman, C.W., 2009. Raster-based analysis of coastal terrain dynamics from multitemporal lidar Data. J. Coast. Res. 252, 507–514. https://doi.org/10.2112/07-0976.1.
Mitasova, H., Hardin, E., Overton, M.F., Kurum, M.O., 2010. Geospatial analysis of vulnerable beach-foredune systems from decadal time series of LiDAR data. J. Coast. Conserv. 14, 161–172. https://doi.org/10.1007/s11852-010-0088-1.
Montreuil, A.L., Levoy, F., Bretel, P., Anthony, E.J., 2014. Morphological diversity and complex sediment recirculation on the ebb delta of a macrotidal inlet (Normandy, France): a multiple LiDAR dataset approach. Geomorphology 219, 114–125. https://doi.org/10.1016/j.geomorph.2014.05.008.
Mora, O.E., Toth, C.K., 2014. A probabilistic approach to landslide susceptibility mapping using multi-temporal airborne LiDAR data. In: ASPRS 2014 Annual Conference. American Society for Photogrammetry and Remote Sensing, Louisville, Kentucky.
Moretto, J., Rigon, E., Mao, L., Delai, F., Picco, L., Lenzi, M.A., 2014. Short-term geomorphic analysis in a disturbed fluvial environment by fusion of LiDAR, colour bathymetry and dGPS surveys. Catena 122, 180–195. https://doi.org/10.1016/j.catena.2014.06.023.
Mukoyama, S., 2011. Estimation of ground deformation caused by the earthquake (M7.2) in Japan, 2008, from the geomorphic image analysis of high resolution LiDAR DEMs. J. Mt. Sci. 8, 239–245. https://doi.org/10.1007/s11629-011-2106-7.
Murakami, H., Nakagawa, K., Hasegawa, H., Shibata, T., Iwanami, E., 1999. Change detection of buildings using an airborne laser scanner. ISPRS J. Photogramm. Remote Sens. 54, 148–152. https://doi.org/10.1016/S0924-2716(99)00006-4.
Myronenko, A., Song, Xubo, 2010. Point set registration: coherent point drift. IEEE Trans. Pattern Anal. Mach. Intell. 32, 2262–2275. https://doi.org/10.1109/TPAMI.2010.46.
Næsset, E., Bollandsås, O.M., Gobakken, T., Gregoire, T.G., Ståhl, G., 2013. Model-assisted estimation of change in forest biomass over an 11year period in a sample survey supported by airborne LiDAR: a case study with post-stratification to provide “activity data”. Remote Sens. Environ. 128, 299–314. https://doi.org/10.1016/j.rse.2012.10.008.
Næsset, E., Bollandsås, O.M., Gobakken, T., Solberg, S., McRoberts, R.E., 2015. The effects of field plot size on model-assisted estimation of aboveground biomass change using multitemporal interferometric SAR and airborne laser scanning data. Remote Sens. Environ. 168, 252–264. https://doi.org/10.1016/j.rse.2015.07.002.
Neri, M., Mazzarini, F., Tarquini, S., Bisson, M., Isola, I., Behncke, B., Pareschi, M.T., 2008. The changing face of Mount Etna's summit area documented with LiDAR technology. Geophys. Res. Lett. 35, 1–6. https://doi.org/10.1029/2008GL033740.
Nissen, E., Krishnan, A.K., Arrowsmith, J.R., Saripalli, S., 2012. Three-dimensional surface displacements and rotations from differencing pre-and post-earthquake LiDAR point clouds. Geophys. Res. Lett. 39, 1–6. https://doi.org/10.1029/2012GL052460.
Nissen, E., Maruyama, T., Arrowsmith, J.R., Elliott, J.R., Krishnan, A.K., Oskin, M.E., Saripalli, S., 2014. Coseismic fault zone deformation revealed with differential lidar: examples from Japanese Mw ~7 intraplate earthquakes. Earth Planet. Sci. Lett. 405, 244–256. https://doi.org/10.1016/j.epsl.2014.08.031.
Obu, J., Lantuit, H., Grosse, G., Günther, F., Sachs, T., Helm, V., Fritz, M., 2017. Coastal erosion and mass wasting along the Canadian Beaufort Sea based on annual airborne LiDAR elevation data. Geomorphology 293, 331–346. https://doi.org/10.1016/j.geomorph.2016.02.014.
Økseter, R., Bollandsås, O.M., Gobakken, T., Næsset, E., 2015. Modeling and predicting aboveground biomass change in young forest using multi-temporal airborne laser

scanner data. Scand. J. For. Res. 30, 458–469. https://doi.org/10.1080/02827581.2015.1024733.
Okyay, U., Telling, J.W., Glennie, C.L., 2018. Glacial surface feature identification using multispectral airborne laser scanning data. In: Abstract G51B-482O Presented at 2018 Fall Meeting. AGU.
Orem, C.A., Pelletier, J.D., 2015. Quantifying the time scale of elevated geomorphic response following wildfires using multi-temporal LiDAR data: an example from the Las Conchas fire, Jemez Mountains, New Mexico. Geomorphology 232, 224–238. https://doi.org/10.1016/j.geomorph.2015.01.006.
Oskin, M.E., Arrowsmith, J.R., Hinojosa-Corona, A., Elliott, A.J., Fletcher, J.M., Fielding, E.J., Gold, P.O., Garcia, J.J.G., Hudnut, K.W., Liu-Zeng, J., Teran, O.J., 2012. Near-field deformation from the El Mayor-Cucapah earthquake revealed by differential LiDAR. Science 335, 702–705. https://doi.org/10.1126/science.1213778.
Painter, T.H., Berisford, D.F., Boardman, J.W., Bormann, K.J., Deems, J.S., Gehrke, F., Hedrick, A., Joyce, M., Laidlaw, R., Marks, D., Mattmann, C., McGurk, B., Ramirez, P., Richardson, M., Skiles, S.M.K., Seidel, F.C., Winstral, A.H., 2016. The Airborne Snow Observatory: fusion of scanning lidar, imaging spectrometer, and physically-based modeling for mapping snow water equivalent and snow albedo. Remote Sens. Environ. 184, 139–152. https://doi.org/10.1016/j.rse.2016.06.018.
Passalacqua, P., Belmont, P., Staley, D.M., Simley, J.D., Arrowsmith, J.R., Bode, C.A., Crosby, C., DeLong, S.B., Glenn, N.F., Kelly, S.A., Lague, D., Sangireddy, H., Schaffrath, K.R., Tarboton, D.G., Wasklewicz, T., Wheaton, J.M., 2015. Analyzing high resolution topography for advancing the understanding of mass and energy transfer through landscapes: a review. Earth Sci. Rev. 148, 174–193. https://doi.org/10.1016/j.earscirev.2015.05.012.
Pawłuszek, K., Borkowski, A., 2017. Automatic landslides mapping in the principal component domain. In: Mikoš, M., Vilímek, V., Yin, Y., Sassa, K. (Eds.), Advancing Culture of Living with Landslides. vol. 2017. Springer, Cham, Ljubljana, Slovenia, pp. 421–428. https://doi.org/10.1007/978-3-319-53483-1_50. World Landslide Forum.
Pelletier, J.D., Orem, C.A., 2014. How do sediment yields from post-wildfire debris-laden flows depend on terrain slope, soil burn severity class, and drainage basin area? Insights from airborne-LiDAR change detection. Earth Surf. Process. Landf. 39, 1822–1832. https://doi.org/10.1002/esp.3570.
Pomerleau, F., Colas, F., Siegwart, R., Magnenat, S., 2013. Comparing ICP variants on real-world data sets: open-source library and experimental protocol. Auton. Robot. 34, 133–148. https://doi.org/10.1007/s10514-013-9327-2.
Pye, K., Blott, S.J., 2016. Assessment of beach and dune erosion and accretion using LiDAR: Impact of the stormy 2013-14 winter and longer term trends on the Sefton Coast, UK. Geomorphology 266, 146–167. https://doi.org/10.1016/j.geomorph.2016.05.011.
Qin, R., Tian, J., Reinartz, P., 2016. 3D change detection – Approaches and applications. ISPRS J. Photogramm. Remote Sens. 122, 41–56. https://doi.org/10.1016/j.isprsjprs.2016.09.013.
Reddy, A.D., Hawbaker, T.J., Wurster, F., Zhu, Z., Ward, S., Newcomb, D., Murray, R., 2015. Quantifying soil carbon loss and uncertainty from a peatland wildfire using multi-temporal LiDAR. Remote Sens. Environ. 170, 306–316. https://doi.org/10.1016/j.rse.2015.09.017.
Reitz, M.D., Jerolmack, D.J., Ewing, R.C., Martin, R.L., 2010. Barchan-parabolic dune pattern transition from vegetation stability threshold. Geophys. Res. Lett. 37, 1–5. https://doi.org/10.1029/2010GL044957.
Réjou-Méchain, M., Tymen, B., Blanc, L., Fauset, S., Feldpausch, T.R., Monteagudo, A., Phillips, O.L., Richard, H., Chave, J., 2015. Using repeated small-footprint LiDAR acquisitions to infer spatial and temporal variations of a high-biomass Neotropical forest. Remote Sens. Environ. 169, 93–101. https://doi.org/10.1016/j.rse.2015.08.001.
Renslow, M.S. (Ed.), 2012. Manual of Airborne Topographic Lidar. American Society for Photogrammetry and Remote Sensing, Bethesda, MD.
Richter, R., Döllner, J., 2014. Concepts and techniques for integration, analysis and visualization of massive 3D point clouds. Comput. Environ. Urban Syst. 45, 114–124. https://doi.org/10.1016/j.compenvurbsys.2013.07.004.
Richter, A., Faust, D., Maas, H.G., 2013a. Dune cliff erosion and beach width change at the northern and southern spits of Sylt detected with multi-temporal LiDAR. Catena 103, 103–111. https://doi.org/10.1016/j.catena.2011.02.007.
Richter, R., Kyprianidis, J.E., Döllner, J., 2013b. Out-of-core gpu-based change detection in massive 3D point clouds. Trans. GIS 17, 724–741. https://doi.org/10.1111/j.1467-9671.2012.01362.x.
Rieg, L., Wichmann, V., Rutzinger, M., Sailer, R., Geist, T., Stötter, J., 2014. Data infrastructure for multitemporal airborne LiDAR point cloud analysis - examples from physical geography in high mountain environments. Comput. Environ. Urban Syst. 45, 137–146. https://doi.org/10.1016/j.compenvurbsys.2013.11.004.
Rusinkiewicz, S., Levoy, M., 2001. Efficient variants of the ICP algorithm. In: Proceedings Third International Conference on 3-D Digital Imaging and Modeling. IEEE, pp. 145–152. https://doi.org/10.1109/IM.2001.924423.
Sailer, R., Bollmann, E., Hoinkes, S., Rieg, L., Sproß, M., Stötter, J., 2012. Quantification of geomorphodynamics in glaciated and recently deglaciated terrain based on airborne laser scanning data. Geogr. Ann. Ser. A Phys. Geogr. 94, 17–32. https://doi.org/10.1111/j.1468-0459.2012.00456.x.
Schaffrath, K.R., Belmont, P., Wheaton, J.M., 2015. Landscape-scale geomorphic change detection: quantifying spatially variable uncertainty and circumventing legacy data issues. Geomorphology 250, 334–348. https://doi.org/10.1016/j.geomorph.2015.09.020.
Schmaltz, E.M., Steger, S., Glade, T., 2017. The influence of forest cover on landslide occurrence explored with spatio-temporal information. Geomorphology 290, 250–264. https://doi.org/10.1016/j.geomorph.2017.04.024.
Schöber, J., Schneider, K., Helfricht, K., Schattan, P., Achleitner, S., Schöberl, F., Kirnbauer, R., 2014. Snow cover characteristics in a glacierized catchment in the Tyrolean Alps - improved spatially distributed modelling by usage of LiDAR data. J. Hydrol. 519, 3492–3510. https://doi.org/10.1016/j.jhydrol.2013.12.054.
Scott, C.P., Arrowsmith, J.R., Nissen, E., Lajoie, L., Maruyama, T., Chiba, T., 2018. The M7 2016 Kumamoto, Japan, earthquake: 3-D deformation along the Fault and within the damage zone constrained from differential lidar topography. J. Geophys. Res. Solid Earth 123, 6138–6155. https://doi.org/10.1029/2018JB015581.
Shan, J., Toth, C.K. (Eds.), 2008. Topographic Laser Ranging and Scanning: Principles and Processing. CRC Press, Boca Raton, FL.
Sherman, D.J., Hales, B.U., Potts, M.K., Ellis, J.T., Liu, H., Houser, C., 2013. Impacts of Hurricane Ike on the beaches of the Bolivar Peninsula, TX, USA. Geomorphology 199, 62–81. https://doi.org/10.1016/j.geomorph.2013.06.011.
Simonson, W., Ruiz-Benito, P., Valladares, F., Coomes, D., 2016. Modelling above-ground carbon dynamics using multi-temporal airborne lidar: insights from a Mediterranean woodland. Biogeosciences 13, 961–973. https://doi.org/10.5194/bg-13-961-2016.
Singh, A., 1989. Digital change detection techniques using remotely-sensed data. Int. J. Remote Sens. 10, 989–1003. https://doi.org/10.1080/01431168908903939.
Skowronski, N.S., Clark, K.L., Gallagher, M., Birdsey, R.A., Hom, J.L., 2014. Airborne laser scanner-assisted estimation of aboveground biomass change in a temperate oak-pine forest. Remote Sens. Environ. 151, 166–174. https://doi.org/10.1016/j.rse.2013.12.015.
Starek, M.J., Vemula, R., Slatton, K.C., 2012. Probabilistic detection of morphologic indicators for beach segmentation with multi-temporal LiDAR measurements. IEEE Trans. Geosci. Remote Sens. 50, 4759–4770. https://doi.org/10.1109/TGRS.2012.2191559.
Starek, M.J., Cu, T., Bridges, D., 2018. Evaluation of a survey-grade, long-range Uas lidar system: a case study in South Texas, USA. In: IEEE International Geoscience and Remote Sensing Symposium, IGARSS. IEEE, pp. 8765–8768. https://doi.org/10.1109/IGARSS.2018.8517340.
Tarolli, P., 2014. High-resolution topography for understanding Earth surface processes: opportunities and challenges. Geomorphology 216, 295–312. https://doi.org/10.1016/j.geomorph.2014.03.008.
Telling, J.W., Glennie, C.L., Fountain, A.G., Finnegan, D.C., 2017. Analyzing glacier surface motion using LiDAR data. Remote Sens. 9, 9–12. https://doi.org/10.3390/rs9030283.
Tennant, C.J., Harpold, A.A., Lohse, K.A., Godsey, S.E., Crosby, B.T., Larsen, L.G., Brooks, P.D., Van Kirk, R.W., Glenn, N.F., 2017. Regional sensitivities of seasonal snowpack to elevation, aspect, and vegetation cover in western North America. Water Resour. Res. 53, 6908–6926. https://doi.org/10.1002/2016WR019374.
Tinkham, W.T., Smith, A.M.S., Marshall, H.-P.P., Link, T.E., Falkowski, M.J., Winstral, A.H., 2014. Quantifying spatial distribution of snow depth errors from LiDAR using random forest. Remote Sens. Environ. 141, 105–115. https://doi.org/10.1016/j.rse.2013.10.021.
Tran, T.H.G., Ressl, C., Pfeifer, N., 2018. Integrated change detection and classification in urban areas based on airborne laser scanning point clouds. Sensors 18. https://doi.org/10.3390/s18020448.
Tseng, C.-M., Lin, C.-W., Stark, C.P., Liu, J.K., Fei, L.Y., Hsieh, Y.C., 2013. Application of a multi-temporal, LiDAR-derived, digital terrain model in a landslide-volume estimation. Earth Surf. Process. Landf. 38, 1587–1601. https://doi.org/10.1002/esp.3454.
Tseng, C.-M., Lin, C.-W., Dalla Fontana, G., Tarolli, P., 2015. The topographic signature of a major typhoon. Earth Surf. Process. Landf. 40, 1129–1136. https://doi.org/10.1002/esp.3708.
USGS, 2018a. Kilauea Volcano, HI June 2018 Acquisition airborne lidar survey. U.S. Geological Survey (USGS) in collaboration with GEO1, Winward Aviation, Quantum Spatial, and Cold Regions Research and Engineering Laboratory, distributed by OpenTopography. https://doi.org/10.5069/G98K7718.
USGS, 2018b. Kilauea Volcano, HI July 2018 Acquisition Airborne Lidar Survey. U.S. Geological Survey (USGS) in Collaboration with the State of Hawaii. Federal Emergency Management Agency, Cold Regions Research and Engineering Laboratory, and the National Center for Aihttps://doi.org/10.5069/G9M32SV1.
Vehling, L., Baewert, H., Glira, P., Moser, M., Rohn, J., Morche, D., 2017. Quantification of sediment transport by rockfall and rockslide processes on a proglacial rock slope (Kaunertal, Austria). Geomorphology 287, 46–57. https://doi.org/10.1016/j.geomorph.2016.10.032.
Ventura, G., Vilardo, G., Terranova, C., Sessa, E.B., 2011. Tracking and evolution of complex active landslides by multi-temporal airborne LiDAR data: the Montaguto landslide (Southern Italy). Remote Sens. Environ. 115, 3237–3248. https://doi.org/10.1016/j.rse.2011.07.007.
Vericat, D., Wheaton, J.M., Brasington, J., 2017. Revisiting the morphological approach. In: Tsutsumi, D., Laronne, J. (Eds.), Gravel-Bed Rivers: Processes and Disasters. John Wiley & Sons Ltd, Chichester, UK, pp. 121–158. https://doi.org/10.1002/9781118971437.ch5.
Vo, A.V., Laefer, D.F., Bertolotto, M., 2016. Airborne laser scanning data storage and indexing: state-of-the-art review. Int. J. Remote Sens. 37, 6187–6204. https://doi.org/10.1080/01431161.2016.1256511.
Wagner, W., Lague, D., Mohrig, D., Passalacqua, P., Shaw, J., Moffett, K., 2017. Elevation change and stability on a prograding delta. Geophys. Res. Lett. 44, 1786–1794. https://doi.org/10.1002/2016GL072070.
Wheaton, J.M., 2008. Uncertainty in Morphological Sediment Budgeting of Rivers (PhD Dissertation). University of Southampton.
Wheaton, J.M., Brasington, J., Darby, S.E., Sear, D.A., 2010. Accounting for uncertainty in DEMs from repeat topographic surveys: improved sediment budgets. Earth Surf. Process. Landf. 35, 136–156. https://doi.org/10.1002/esp.1886.
White, S.A., Wang, Y., 2003. Utilizing DEMs derived from LiDAR data to analyze morphologic change in the North Carolina coastline. Remote Sens. Environ. 85, 39–47. https://doi.org/10.1016/S0034-4257(02)00185-2.
Wicherski, W., Dethier, D.P., Ouimet, W.B., 2017. Erosion and channel changes due to

extreme flooding in the Fourmile Creek catchment, Colorado. Geomorphology 294, 87–98. https://doi.org/10.1016/j.geomorph.2017.03.030.
Woolard, J.W., Colby, J.D., 2002. Spatial characterization, resolution, and volumetric change of coastal dunes using airborne LIDAR: Cape Hatteras, North Carolina. Geomorphology 48, 269–287. https://doi.org/10.1016/S0169-555X(02)00185-X.
Wu, B., Guo, J., Hu, H., Li, Z., Chen, Y., 2013. Co-registration of lunar topographic models derived from Chang'E-1, SELENE, and LRO laser altimeter data based on a novel surface matchingmethod. Earth Planet. Sci. Lett. 364, 68–84. https://doi.org/10.1016/j.epsl.2012.12.024.
Wulder, M.A., Coops, N.C., 2014. Make earth observations open access. Nature 513, 30–31. https://doi.org/10.1038/513030a.
Wulder, M.A., White, J.C., Alvarez, F., Han, T., Rogan, J., Hawkes, B., 2009. Characterizing boreal forest wildfire with multi-temporal Landsat and LIDAR data. Remote Sens. Environ. 113, 1540–1555. https://doi.org/10.1016/j.rse.2009.03.004.
Wulder, M.A., White, J.C., Nelson, R.F., Næsset, E., Orka, H.O., Coops, N.C., Hilker, T., Bater, C.W., Gobakken, T., Næsset, E., Ørka, H.O., Coops, N.C., Hilker, T., Bater, C.W., Gobakken, T., Orka, H.O., Coops, N.C., Hilker, T., Bater, C.W., Gobakken, T., Næsset, E., Ørka, H.O., Coops, N.C., Hilker, T., Bater, C.W., Gobakken, T., 2012. LiDAR sampling for large-area forest characterization: a review. Remote Sens. Environ. 121, 196–209. https://doi.org/10.1016/j.rse.2012.02.001.
Xu, H., Cheng, L., Li, M., Chen, Y., Zhong, L., 2015. Using octrees to detect changes to buildings and trees in the urban environment from airborne LiDAR data. Remote Sens. 7, 9682–9704. https://doi.org/10.3390/rs70809682.
Young, A.P., Ashford, S.A., 2006. Application of airborne LiDAR for seacliff volumetric change and beach-sediment budget contributions. J. Coast. Res. 222, 307–318. https://doi.org/10.2112/05-0548.1.
Zhang, X., Glennie, C.L., Kusari, A., 2015. Change detection from differential airborne LiDAR using a weighted anisotropic Iterative Closest Point algorithm. IEEE J. Sel. Top. Appl. Earth Obs. Remote Sens. 8, 3338–3346. https://doi.org/10.1109/JSTARS.2015.2398317.
Zhou, G., Xie, M., 2009. Coastal 3-D morphological change analysis using LiDAR series data: a case study of Assateague Island National Seashore. J. Coast. Res. 25, 435–447. https://doi.org/10.2112/07-0985.1.
Zhu, Z., 2017. Change detection using landsat time series: a review of frequencies, preprocessing, algorithms, and applications. ISPRS J. Photogramm. Remote Sens. 130, 370–384. https://doi.org/10.1016/j.isprsjprs.2017.06.013.